

NBSIR 75-806

**PHASE EQUILIBRIUM AND FLOW-INDUCED DESORPTION DATA
FOR He-CO, He-N₂O, AND He-N₂ SYSTEMS**

W. G. Steward
R. O. Voth
J. Hord
W. R. Parrish
C. F. Sindt
J. M. Arvidson

Cryogenics Division
Institute for Basic Standards
National Bureau of Standards
Boulder, Colorado 80302

March 1975

Prepared for
Kirtland Air Force Base
Albuquerque, New Mexico 87117

NBSIR 75-806

PHASE EQUILIBRIUM AND FLOW-INDUCED DESORPTION DATA FOR He-CO, He-N₂O, AND He-N₂ SYSTEM

W. G. Steward
R. O. Voth
J. Hord
W. R. Parrish
C. F. Sindt
J. M. Arvidson

Cryogenics Division
Institute for Basic Standards
National Bureau of Standards
Boulder, Colorado 80302

March 1975

Prepared for
Kirtland Air Force Base
Albuquerque, New Mexico 87117



U.S. DEPARTMENT OF COMMERCE, Frederick B. Dent, Secretary

NATIONAL BUREAU OF STANDARDS, Richard W. Roberts, Director

CONTENTS

	Page
Nomenclature	vii
1. Introduction	1
2. Phase Equilibrium Experiments	2
2.1 Experimental Method	2
2.2 Results and Discussion	4
3. Scale Model Flow-Induced Desorption Tests	20
3.1 Scaling Criteria	20
3.2 Instrumentation	22
3.3 Test Procedure	22
3.4 Results and Discussion	23
3.4.1 Head Meter Flow Coefficient	24
3.4.2 Resistive Flow	25
3.4.3 Cavitating Venturi Flow	28
3.5 Experimental Observations	42
4. Conclusions	42
5. References	44
Appendix A1	45
Appendix A2	49

LIST OF FIGURES

Figure	Page
1. Pseudo Henry's Law constant for the He-CO system as a function of pressure	7
2. Pseudo Henry's Law constant for the He-CO system as a function of temperature	8
3. Enhancement factor for the He-CO system as a function of pressure	14
4. Enhancement factor for the He-CO system as a function of temperature	15

5.	Pseudo Henry's Law constant for the He-N ₂ O system as a function of pressure	16
6.	Pseudo Henry's Law constant for the He-N ₂ O system as a function of temperature	17
7.	Enhancement factor for the He-N ₂ O system as a function of pressure	18
8.	Enhancement factor for the He-N ₂ O system as a function of temperature	19
9.	Flow induced desorption test apparatus	21
10.	Adaptation of Martinelli and Nelson [9] correlation for two-phase flow resistance assuming no slip and both phases turbulent	26
11.	Axial pressure gradient as a function of local pressure for He-N ₂ O flow rate of 759 g/s-cm ² (1555 lb/s-ft ²) and initial pressure of 75.8 bars (1100 psia)	27
12.	Overall pressure drop. Comparison between equilibrium flow of saturated N ₂ O and pure liquid	29
13.	Flow rate indication as a function of nozzle upstream pressure for liquid nitrogen at 80.3 K (145°R).	31
14.	Flow rate indication as a function of nozzle upstream pressure for liquid carbon monoxide at 85.3 K (153°R)	32
15.	Flow rate indication as a function of nozzle upstream pressure for liquid nitrous oxide at 255 K (459°R).	33
16.	Flow rate indication as a function of nozzle upstream pressure for liquid nitrous oxide at 266 K (479°R).	34
17.	Flow rate indication as a function of nozzle upstream pressure for liquid nitrous oxide at 244 K (439°R)	35
18.	Cavitation parameter as a function of nozzle pressure drop parameter for liquid nitrogen at 80.3 K (145°R)	37
19.	Cavitation parameter as a function of nozzle pressure drop parameter for liquid carbon monoxide at 85.3 K (153°R)	38
20.	Cavitation parameter as a function of nozzle pressure drop parameter for liquid nitrous oxide at 255 K (459°R).	39

21.	Cavitation parameter as a function of nozzle pressure drop parameter for liquid nitrous oxide at 266 K (479°R) . .	40
22.	Cavitation parameter as a function of nozzle pressure drop parameter for liquid nitrous oxide at 244 K (439°R)	41

LIST OF TABLES

Table		Page
1.	He-CO liquid phase compositions	5
2.	He-CO vapor phase compositions	6
3.	He-N ₂ O liquid phase compositions	11-12
4.	He-N ₂ O vapor phase compositions	13
5.	Homogeneous equilibrium choking flow for He-N ₂ , initial pressure 130 bars (1890 psia). temperature 77 K (138°R)	30
6.	Reduction of flow rate due to helium saturation	36
A1.	Early test results - Nitrogen	46
	Early test results - Carbon Monoxide	47-48
A2.	Final test results - Carbon Monoxide	50
	Final test results - Nitrogen	51
	Final test results - Nitrous Oxide	52-54

ABSTRACT

Liquid-vapor equilibrium data were obtained for the helium-carbon monoxide and helium-nitrous oxide systems at pressures to 138 bars. Liquid and vapor phase compositions were measured at nominal temperatures of 80, 85, 90, 100, and 120 K (144, 153, 162, 180, and 216°R) for the helium-carbon monoxide system, and at 235, 245, 265, and 285 K (423, 441, 477, and 513°R) for the helium-nitrous oxide system. Internal consistency of the data was checked by using pseudo-Henry's Law constants and enhancement factors.

The effects on flow of helium absorption and subsequent flow-induced desorption were investigated by means of reduced scale model experiments. Friction losses attributable to helium desorption in the long channels proved to be negligible both in experimental measurements and in calculations based on assumed equilibrium of liquid and gas. Contrarily, the assumption of phase equilibrium leads to gross miscalculations of flow rates in cavitating or near cavitating nozzles or venturis. Actual venturi mass flow rates reached in the experiments were fifty times the theoretical choking flow rates; however, definite mass flow rate reductions due to helium desorption were measured, ranging from four percent for nitrogen to twelve percent for nitrous oxide. Pertinent experiences in handling these fluids and operating the test equipment are also discussed.

Key words: Binary mixture; cavitating venturi; enhancement factors; experimental vapor-liquid equilibria; flow induced desorption; helium-carbon monoxide system; helium-nitrous oxide system; Henry's Law constants; two phase choking; two phase flow.

Nomenclature

Phase equilibrium -- Section 2

- E = Enhancement factor, dimensionless.
H = Pseudo Henry's Law constant, bar.
P = Total pressure, bars.
 P^0 = Vapor pressure, bars.
x = Mole fraction in the liquid phase.
y = Mole fraction in the vapor phase.

Subscripts

- 1 = less volatile component.
2 = more volatile component.

Flow induced desorption -- Section 3

- C_d = flow meter discharge coefficient.
 C_v = cavitating venturi discharge coefficient.
 f_{tg} = friction factor as though the total flow were gas.
 f_{tl} = friction factor as though the total flow were liquid.
 f_v = volume fraction of vapor.
G = mass flow per unit area.
 G_{max} = limiting or choking value of G.
P = pressure.
 P_1 = supply pressure.
 P_2 = pressure upstream from the cavitating venturi.
 P_3 = pressure downstream from the cavitating venturi.
 ΔP_4 = flow meter pressure differential.
 P_{sat} = saturation pressure.
Re = Reynold's number.
 v = specific volume.
W = mass flow rate.
 x' = axial length.
Y = mass fraction of vapor or gas.

Nomenclature

Flow induced desorption -- Section 3 (Continued)

- β = two phase properties parameter.
 θ = two phase flow pressure drop factor.
 ρ_l = liquid density.
 ρ_g = gas density.
 μ = viscosity.

PHASE EQUILIBRIUM AND FLOW-INDUCED DESORPTION
DATA FOR He-CO, He-N₂O, and He-N₂ SYSTEMS*

W. G. Steward, R. O. Voth, J. Hord, W. R. Parrish,
C. F. Sindt, and J. M. Arvidson

1. Introduction

Helium gas pressurization often is preferable to the use of pumps for transferring cryogenic liquids; however, there is concern that helium, being soluble in these liquids, might be absorbed under pressure and desorbed in the piping, thereby producing the high pressure drop and choking characteristics of two-phase flow. These problems would be anticipated if phase equilibrium prevailed throughout the flow system, and this would probably disqualify helium pressurization as a practical means of transferring liquids in many applications. Fortunately, perfect phase equilibrium is unlikely in dynamic systems; thus, the actual amount of helium absorbed and desorbed is less than that expected if equilibrium prevailed, particularly where the pressure drop is sudden as in orifices or nozzles. Therefore, designers require not only phase equilibrium data, but also experiments to determine the effects of flow-induced helium desorption in models of specific systems. The systems of concern in this report involve helium pressurized liquid nitrogen, liquid carbon monoxide, and liquid nitrous oxide; reliable phase equilibrium data are lacking for the last two of these fluids and flow induced desorption data are unavailable for any of the fluids. These fluids are of interest because they are candidate propellants for special purpose gas generator systems.

In response to these requirements, this investigation supplies needed data on phase equilibrium of helium with liquid carbon monoxide and liquid nitrous oxide, and flow-induced desorption effects on all three fluids of interest. The experimental program was carried out in two phases:

* This study was performed at the National Bureau of Standards, Boulder, Colorado, under the sponsorship of Kirtland Air Force Base, Albuquerque, New Mexico.

- (1) Phase equilibrium experiments for helium-carbon monoxide and helium-nitrous oxide systems.
- (2) Scaled model tests to determine the effects of helium gas absorption and desorption on pressure drop and flow rates in pipelines and nozzles. These tests are divided into two categories: gradual pressure drop due to friction in tubing and restrictions, and sudden pressure drop in a flow nozzle.

2. Phase Equilibrium Experiments

Cryogenic systems containing helium have been of practical interest for applications ranging from separation processes to pressurized systems. However, few data exist in the literature for helium systems containing carbon monoxide or nitrous oxide. Sinor and Kurata [1] determined liquid phase compositions of helium-carbon monoxide mixtures at four temperatures between 77 and 128 K and at pressures up to 138 bars. Kling [2] made an extensive experimental study of nitrous oxide systems including the helium-nitrous oxide system; however, his data are presented in graphical form only, and the internal consistency of the data could not be assessed. The work reported here was performed to provide a more complete set of phase equilibrium data for these two binary systems.

2.1 Experimental Method

The phase equilibrium apparatus used here is basically the vapor-recirculation system described by Duncan and Hiza [3]; therefore, only pertinent details are given here.

Equilibrium pressures were measured by using either a double revolution 0 to 20 bar Bourdon gauge or a 0 to 2000 psia Bourdon gauge. The 0 to 20 bar gauge, calibrated against an air piston gauge, exhibited a maximum negative deviation of 0.02 bars below 3 bars and a constant negative deviation of 0.008 bars above 8 bars. The 2000 psia gauge, calibrated against an oil dead weight gauge, has an estimated overall uncertainty of 1.0 psi.

The fluid temperatures were measured with a platinum resistance thermometer. Comparisons were made between readings of this thermometer

and temperatures obtained from vapor pressure measurements with pure nitrogen and the vapor pressure data of Wagner [4]. These comparisons, together with the specifications of the measuring instruments, indicate the overall uncertainty of the temperature measurements is no greater than ± 0.013 K.

Liquid phase samples were withdrawn from the bottom of the equilibrium cell through a stainless steel capillary; vapor samples were isolated in the room temperature recirculation loop. To obtain reproducible analyses in the nitrous oxide system liquid samples were slowly bled into a warm, evacuated 75 cm^3 chamber and allowed to reach thermal equilibrium (~ 20 minutes) prior to gas analysis. The same procedure was used for vapor sampling except that it was not necessary to wait before analyzing the sample. In each case the sample chamber was filled to about 2 bars gauge to allow for adequate purging of the gas analysis equipment and to provide at least two analyses.

A gas chromatograph containing a thermal conductivity detector was used to determine mixture compositions. It was not possible to obtain both liquid and vapor analyses during the same run because a different carrier gas and column was required for each phase. For liquid phase analyses argon was used as the carrier gas with a 6 m long molecular sieve column. The chromatograph was calibrated against a 5.17 mole percent helium in argon mixture. Helium carrier gas and a 0.5 m long silica gel column was used for vapor phase analyses. In this case the chromatograph was calibrated against pure carbon monoxide or nitrous oxide, and the response in the peak area was assumed to be linear over the composition range of interest. A previous calibration for nitrogen verified the linearity assumption for this detector. In each case only the peak area of one component and total sample pressure were measured. We used a 0 to 75 psia quartz spiral Bourdon gauge to determine sample pressure. The gauge was calibrated to better than 0.1 percent of the reading using an air dead weight gauge. We estimate that the compositions are accurate to within ± 0.2 mole percent or ± 2 percent, whichever is greater; reproducibility, especially for the carbon monoxide system, was much better.

The carbon monoxide was ultra pure ($> 99.8\%$) and the nitrous oxide was of U.S.P. quality ($> 98\%$) with the major impurities of both being nitrogen and oxygen. No attempt was made to further purify the carbon monoxide; however, after condensing nitrous oxide into the equilibrium cell, the vapor space had to be vented three or four times before the vapor pressure remained constant after venting. This venting also provided additional purification of the nitrous oxide.

Carbon monoxide poses a safety problem because it is toxic and not readily detected since it is odorless, colorless and tasteless. To prevent exposure of personnel to the gas, all vent lines were vented directly outdoors. Before any carbon monoxide was used, the complete system was leak-checked to 138 bars with pure helium. As a further precaution, CO detector badges were worn; these badges are reportedly sensitive to carbon monoxide down to the ppm range.

Nitrous oxide is not considered toxic, but it is an anesthetic. This fluid can explosively autodecompose at high temperature and/or pressure [5]. However, at the operating conditions of this study the only problem with nitrous oxide was that it caused swelling in the recirculation pump diaphragm. Thus, periodic shutdowns for pump overhaul were required.

2.2 Results and Discussion

Tables 1 and 2 give liquid and vapor compositions as a function of pressure for the five isotherms of the helium carbon monoxide system. Measured vapor pressures are included because they differ from the correlation of Hust and Stewart [6]. Figure 1 shows pseudo-Henry's Law constants from our data and from Sinor and Kurata's data. The Henry's Law constant is defined here as

$$H = (P - P_1^0)/x_2. \quad (1)$$

Sinor and Kurata's data were reduced using vapor pressures from Hust and Stewart. Figure 2 shows a cross-plot of Henry's Law constants as a function of temperature for helium pseudo partial pressures $(P - P_1^0)$

Table 1. He-CO liquid phase compositions.

K	Temperature		Pressure		Mole % He
	°R	bars	psia		
79.50	143.1	0.787*	11.41*	0.0	
		41.2	597	0.47	
		41.5	602	0.48	
		69.1	1002	0.77	
		69.4	1007	0.79	
		102.7	1489	1.15	
		103.4	1500	1.16	
		134.9	1956	1.43	
		136.1	1974	1.46	
		84.71	152.5	1.41*	20.40*
69.0	1000			1.05	
69.4	1007			1.07	
102.9	1493			1.52	
103.9	1507			1.52	
135.3	1962			1.85	
136.2	1976			1.86	
90.0	162.0			2.37*	34.35*
		35.6	516	0.72	
		69.4	1006	1.41	
		103.6	1503	2.03	
		135.6	1967	2.53	
		136.9	1985	2.54	
		100.0	180.0	5.41*	78.5*
37.1	538			1.16	
70.1	1017			2.27	
104.3	1513			3.33	
136.9	1985			4.19	
120.0	216.0			18.74*	271.8*
		36.5	530	1.74	
		69.9	1014	4.78	
		105.1	1524	7.67	
		138.0	2002	10.03	

* Vapor pressure.

Table 2. He-CO vapor phase compositions.

K	Temperature		Pressure		Mole % CO
		°R	bars	psia	
80.0		144.0	.830*	12.04*	100.0
			11.9	172	7.96
			13.7	198	6.97
			28.8	417	3.64
			42.3	614	2.68
			56.3	817	2.13
			69.8	1012	1.79
			136.4	1978	1.15
84.71		152.5	1.41*	20.4*	100.0
			6.9	100	12.91
			7.0	101	12.87
			15.2	220	10.54
			28.8	418	6.05
			42.8	621	4.37
			56.4	818	3.51
			70.9	1028	2.97
			104.0	1508	2.28
90.0		162.0	2.37*	34.35*	100.0
			14.6	211	18.73
			26.7	387	10.82
			40.1	582	7.61
			55.6	806	5.87
			71.2	1032	4.85
			104.0	1509	3.72
			137.6	1996	3.11
100.0		180.0	5.41*	78.5*	100.0
			13.4	195	45.29
			27.4	398	24.06
			27.9	405	24.04
			29.3	425	22.88
			39.0	565	18.05
			41.4	601	17.21
			57.0	826	13.32
			69.8	1012	11.37
			70.2	1018	11.35
			103.9	1507	8.46
			131.0	1900	7.26
			131.8	1912	7.25
			132.7	1925	7.19
132.9	1928	7.18			
120.0		216	18.74*	271.8*	100.0
			29.3	425	75.99
			42.5	616	59.47
			56.7	822	49.18
			70.5	1023	41.94
			103.8	1505	32.65
			137.1	1988	27.44

* Vapor pressure.

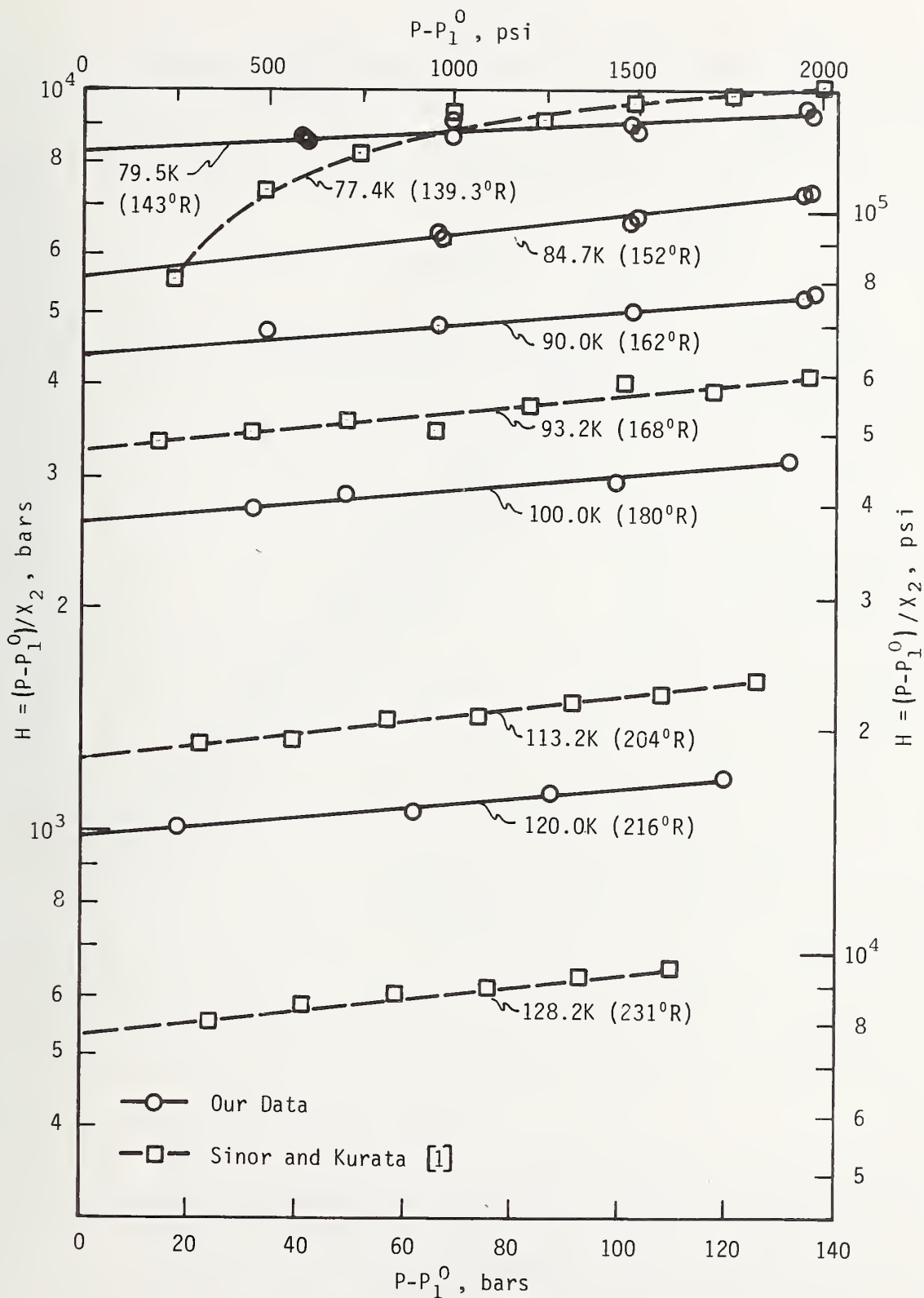


Figure 1. Pseudo Henry's Law constant for the He-CO system as a function of pressure.

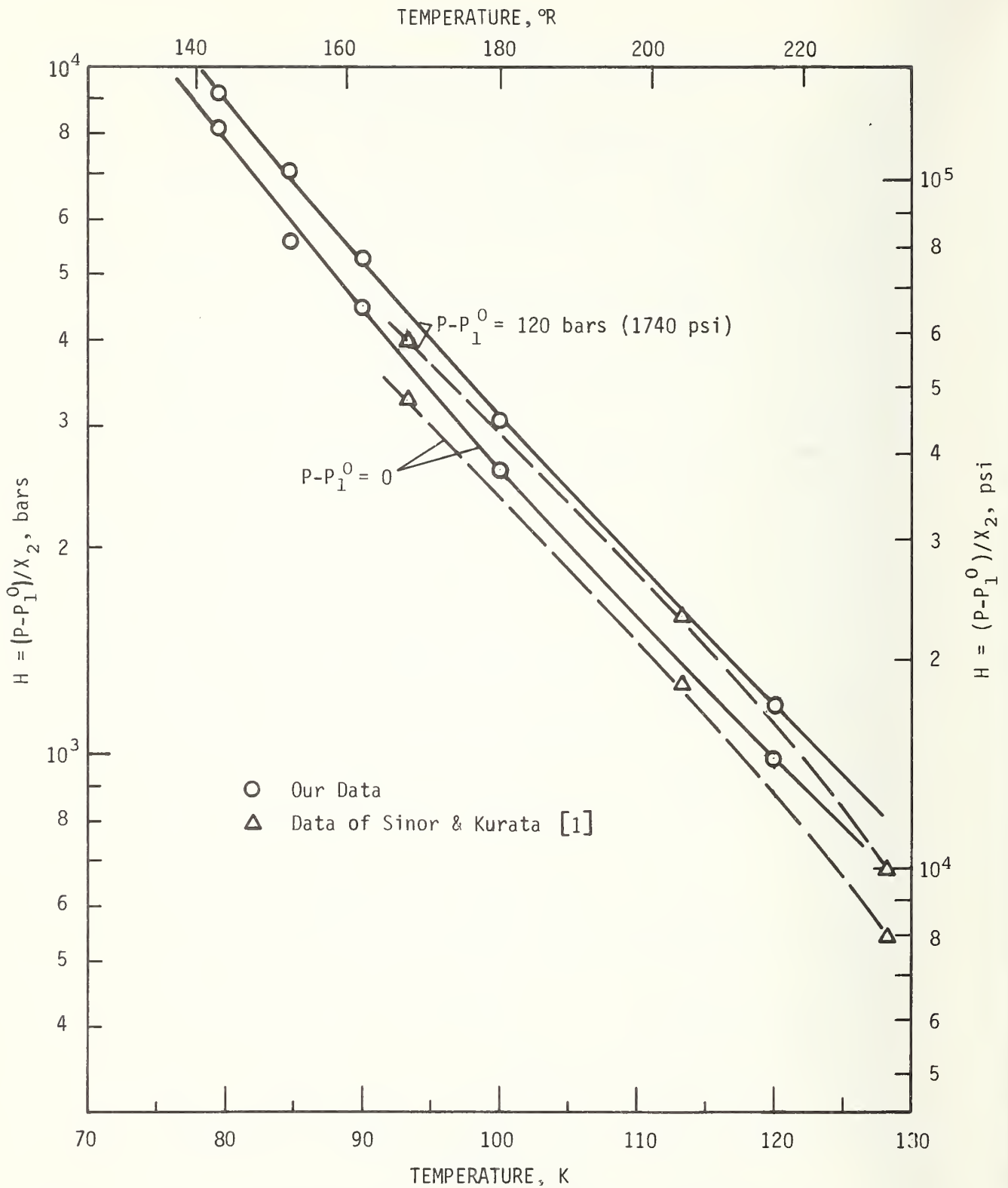


Figure 2. Pseudo Henry's Law constant for the He-CO system as a function of temperature.

of 0 and 120 bars. These figures show a fairly weak pressure dependence for the Henry's Law constant.

A sensitive way to check the consistency of the vapor phase data is to use the enhancement factor which is defined as

$$E \equiv y_1 P / P_1^0. \quad (2)$$

The enhancement factor depends upon the nonidealities of both phases; however, the liquid phase contains only small quantities of solute (He). Therefore, vapor phase nonidealities are the most important contributions to making the enhancement factor greater than unity. Figure 3 shows the enhancement factor as a function of pressure for three of the helium carbon monoxide isotherms. Figure 4 is a cross-plot showing the temperature dependence. The enhancement factor goes through a minimum between 90 and 100 K. The vapor phase data of Buzyna et al. [7] shows a similar minimum in the enhancement factor for the helium-nitrogen system in the same temperature range. The existence of the minimum in the enhancement factor is not fully understood. We do know that it is due to a combination of the slope of the vapor pressure curve, solvent vapor phase nonidealities, and solute-solvent vapor phase nonidealities (He is nearly a perfect gas at these temperatures and pressures).

Liquid and vapor data for the helium-nitrous oxide system are given in tables 3 and 4. Figure 5 shows Henry's Law constants as a function of pressure; within the scatter of the data the Henry's Law constants are independent of pressure. Figure 6 shows a cross-plot of the Henry's Law constant as a function of temperature. Comparisons were not made with Kling's [2] data because the uncertainties involved in reading his graphs make the comparisons meaningless.

Figure 7 shows the enhancement factors for the helium-nitrous oxide system as a function of pressure for three of the isotherms and figure 8 gives the temperature dependence. This system shows no minimum in the enhancement factor because the temperatures are too high. This conclusion

is based on a study of the enhancement factors for the helium-ethane system (ethane and nitrous oxide have similar normal boiling points and critical temperatures) which shows a minimum in the 160 to 190 K range (8). However, figure 8 shows a maximum in the enhancement factors at the lower pressures. The maximum shown in the He-N₂O enhancement factor curve is simpler to explain. It is due to the vapor pressure of N₂O rising more rapidly with temperature than the vapor phase solubility. This also explains the disappearance of the maximum at higher pressures.

Table 3. He-N₂O liquid phase compositions.

K	Temperature		Pressure		Mole % He
		°R	bars	psia	
195.0		351	1.82*	26.40*	0.0
			103.3	1498	0.52
			103.6	1502	0.52
			136.4	1978	0.70
			137.8	1998	0.68
215.0		387.0	4.70*	68.17*	0.0
			49.9	724	0.29
			51.8	751	0.27
			86.1	1248	0.54
235.0		423.0	10.13*	146.92*	0.0
			51.2	742	0.56
			51.6	749	0.55
			84.8	1230	0.96
			86.2	1250	1.04
			136.5	1980	1.70
245.0		441.0	14.14*	205.08*	0.0
			71.0	1030	0.98
			103.2	1497	1.57
			103.7	1504	1.55
			131.3	1904	2.04
			133.9	1942	2.05
			137.6	1996	2.09
			137.8	1998	2.09
			255.0		459.0
38.8	563	0.42			
38.9	564	0.41			
58.2	844	0.87			
58.3	846	0.90			
75.6	1096	1.27			
76.0	1102	1.30			
86.1	1248	1.45			
86.7	1258	1.47			
87.4	1267	1.54			
101.8	1476	1.86			
103.0	1494	1.82			
103.2	1497	1.80			
104.5	1515	1.84			
104.7	1518	1.85			
121.2	1758	2.09			
121.7	1765	2.14			
133.2	1932	2.41			
135.4	1964	2.46			
136.2	1975	2.42			

* Vapor pressure

Table 3. He-N₂O liquid phase compositions (continued).

K	Temperature		Pressure		Mole % He
		°R	bars	psia	
265.0		477.0	25.38*	368*	0.0
			52.5	762	0.77
			52.8	766	0.75
			71.6	1038	1.27
			71.7	1040	1.28
			72.1	1045	1.22
			104.9	1522	2.15
			105.5	1530	2.22
			135.4	1964	2.91
			136.8	1984	2.99
			285.0		513.0
81.8	1186	1.73			
94.3	1367	2.38			
94.6	1372	2.33			
114.6	1662	1.77			
116.9	1695	3.34			
135.5	1965	4.14			
136.1	1974	4.16			
136.7	1983	4.18			

* Vapor pressure

Table 4. He-N₂O vapor phase compositions.

K	Temperature		Pressure		Mole % N ₂ O
	°R	bars	psia		
235.0	423.0	10.13*	146.92*	100.0	
		19.7	285	54.37	
		35.6	516	31.45	
		52.0	754	22.25	
		69.3	1005	17.31	
		104.5	1515	11.81	
		132.9	1928	9.45	
245.0	441.0	14.14*	205.08*	100.0	
		40.3	585	39.93	
		51.7	750	32.20	
		67.6	980	25.30	
		98.2	1424	17.89	
		125.9	1826	14.42	
255.0	459.0	19.22*	278.76*	100.0	
		50.0	739	43.89	
		70.1	1017	33.72	
		103.8	1506	23.70	
		128.5	1863	19.58	
265.0	477.0	25.6	372*	100.0	
		41.6	603	68.72	
		72.5	1052	43.26	
		98.3	1426	33.72	
		99.6	1444	33.30	
		106.0	1538	31.72	
		136.5	1980	25.97	
285.0	513.0	Unable to obtain vapor phase data at this temperature due to rapid failure of circulating pump diaphragms. (Natural rubber and butyl swelled and PTFE, polypyromelitimide and a flouro-elastomeric material failed to maintain suitable elastic properties).			

* Vapor pressure

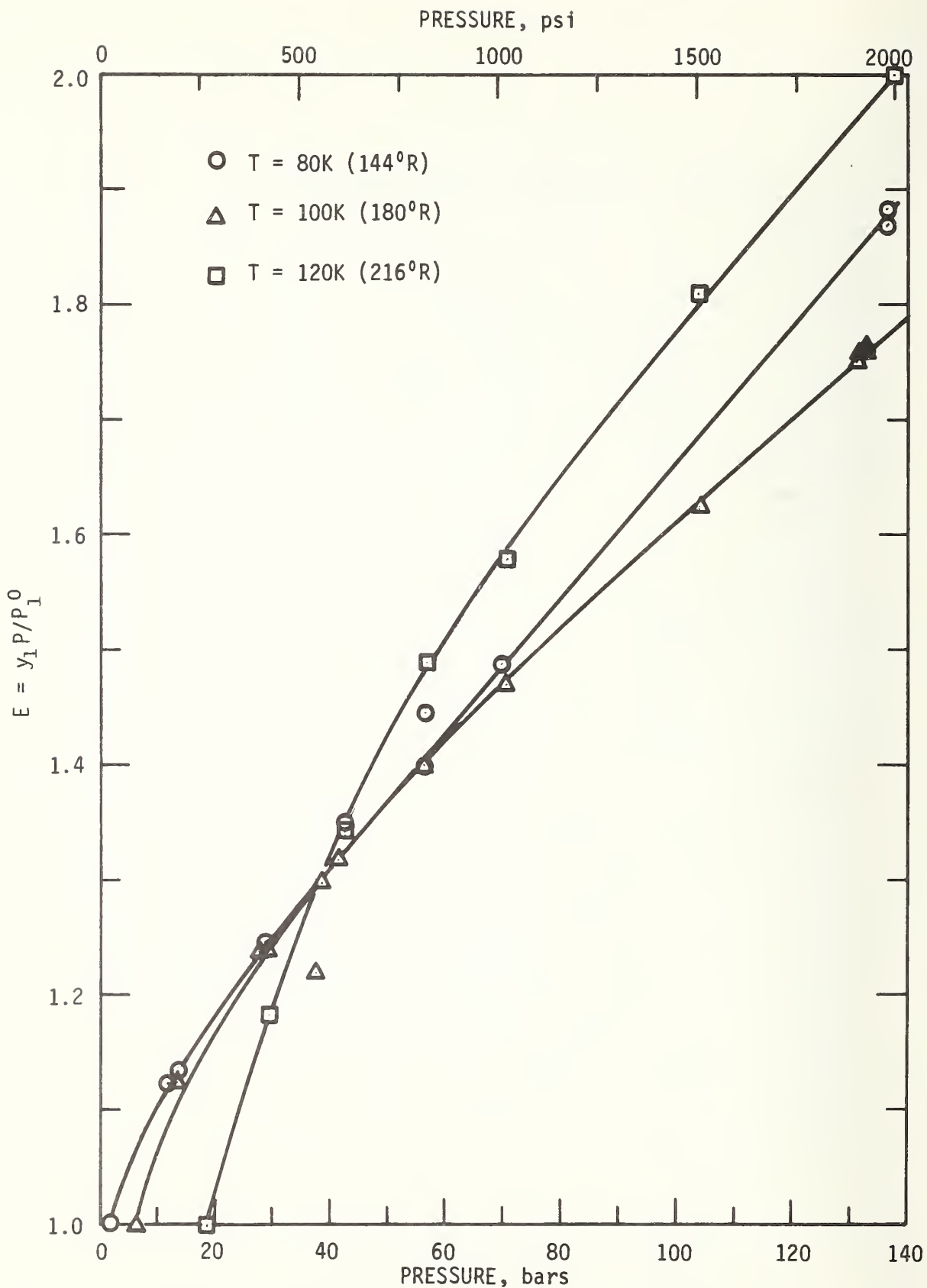


Figure 3. Enhancement factor for the He-CO system as a function of pressure.

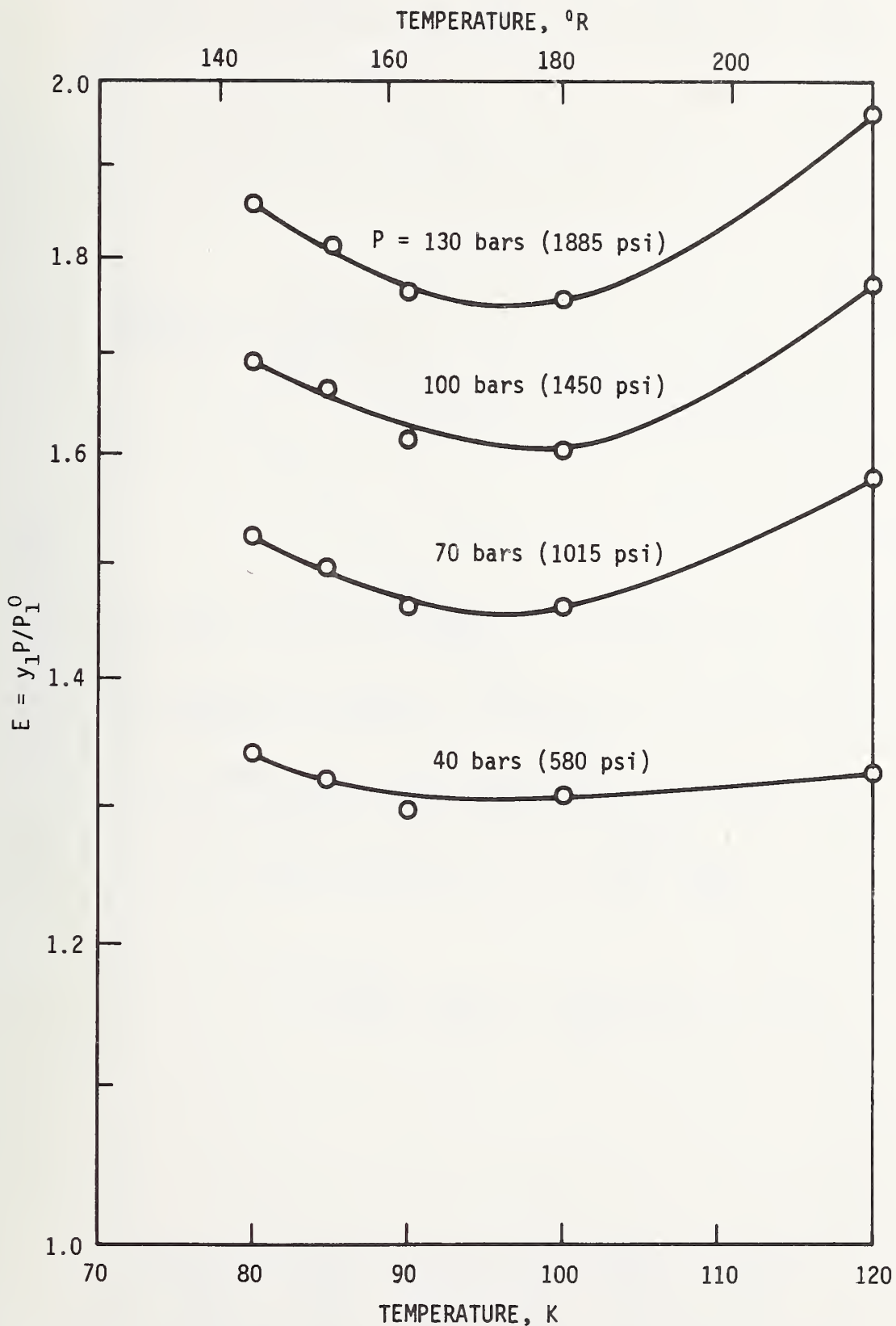


Figure 4. Enhancement factor for the He-CO system as a function of temperature.

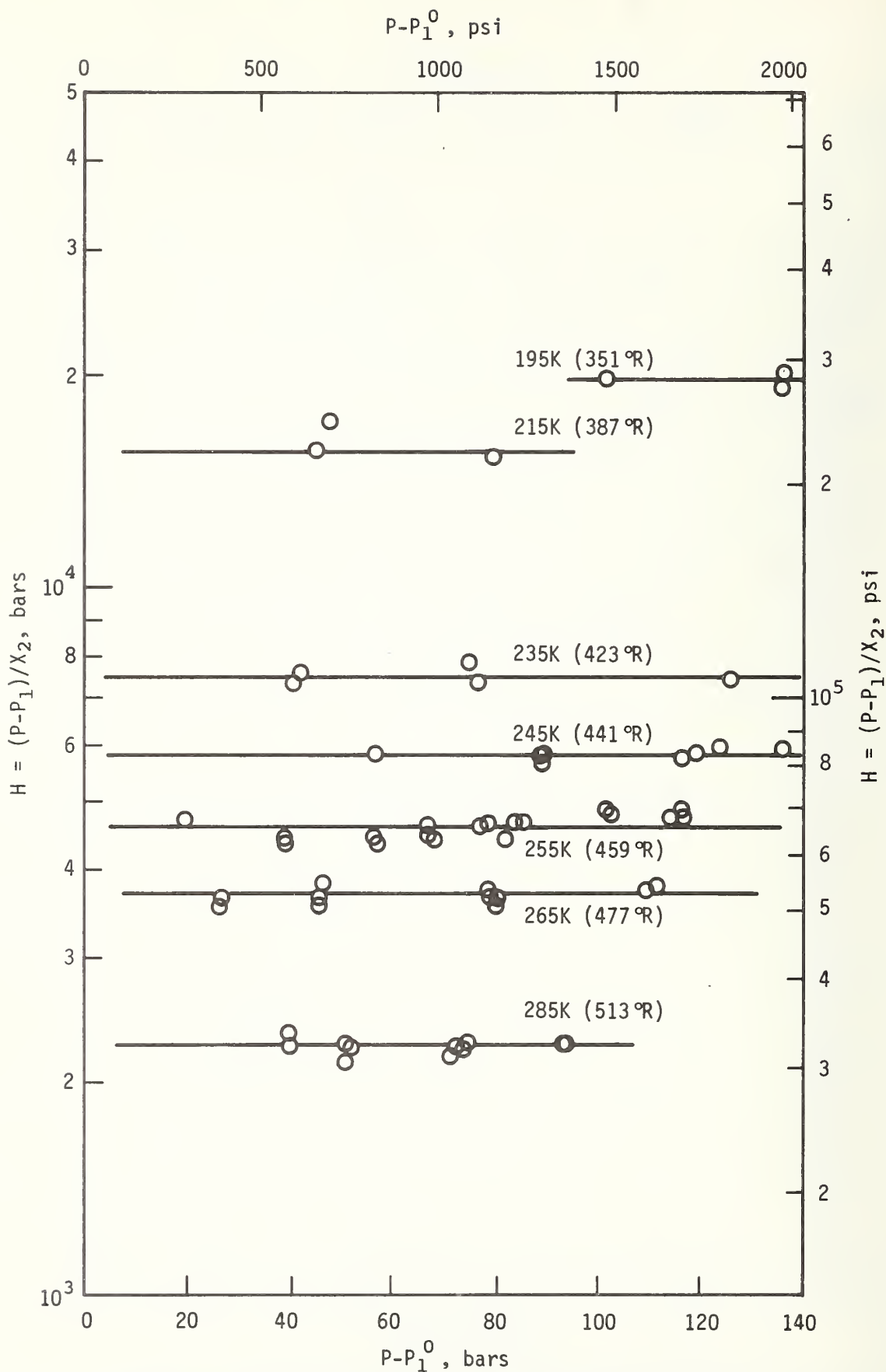


Figure 5. Pseudo Henry's Law constant for the He-N₂O system as a function of pressure.

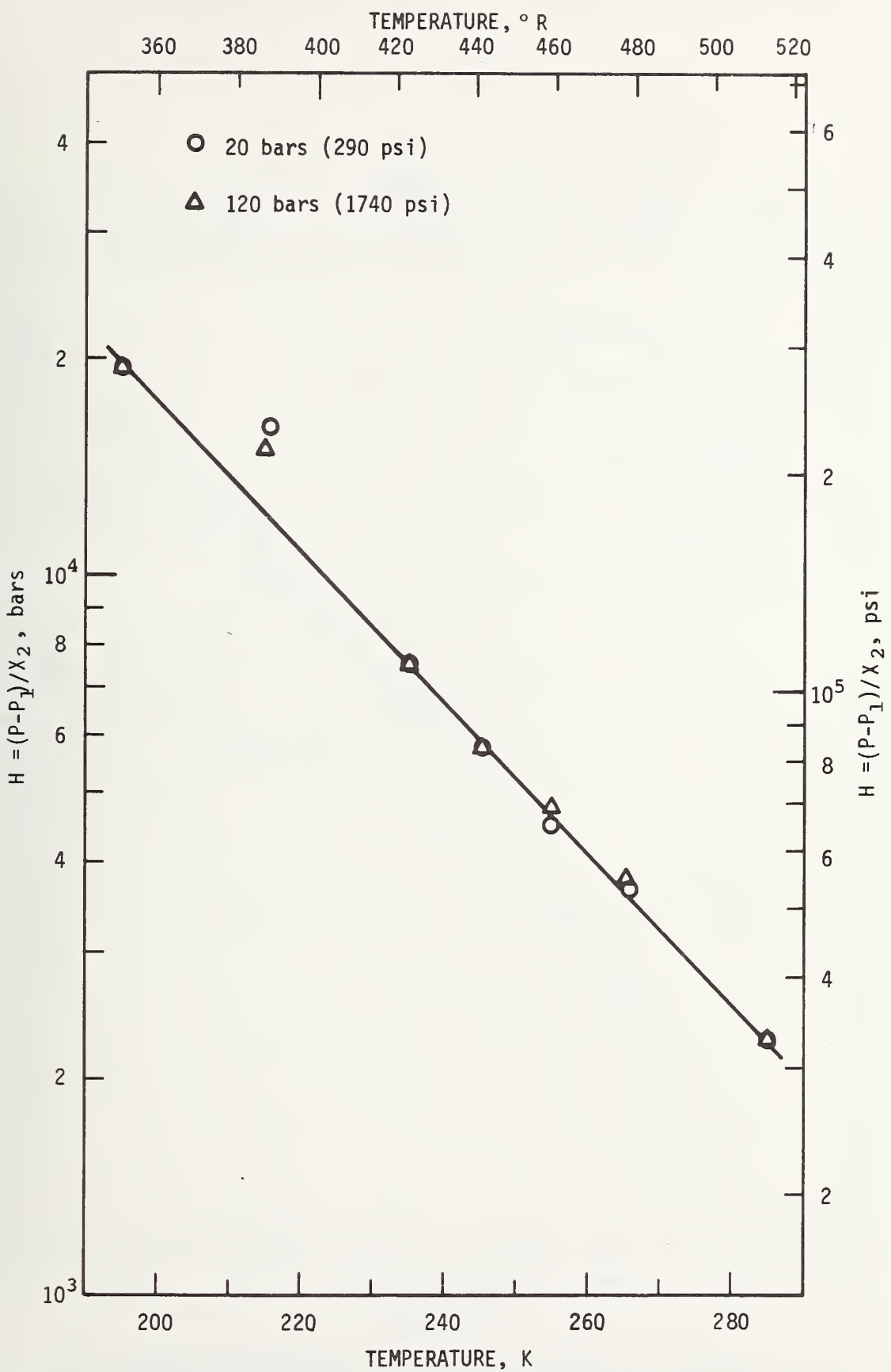


Figure 6. Pseudo Henry's Law constant for the He-N₂O system as a function of temperature.

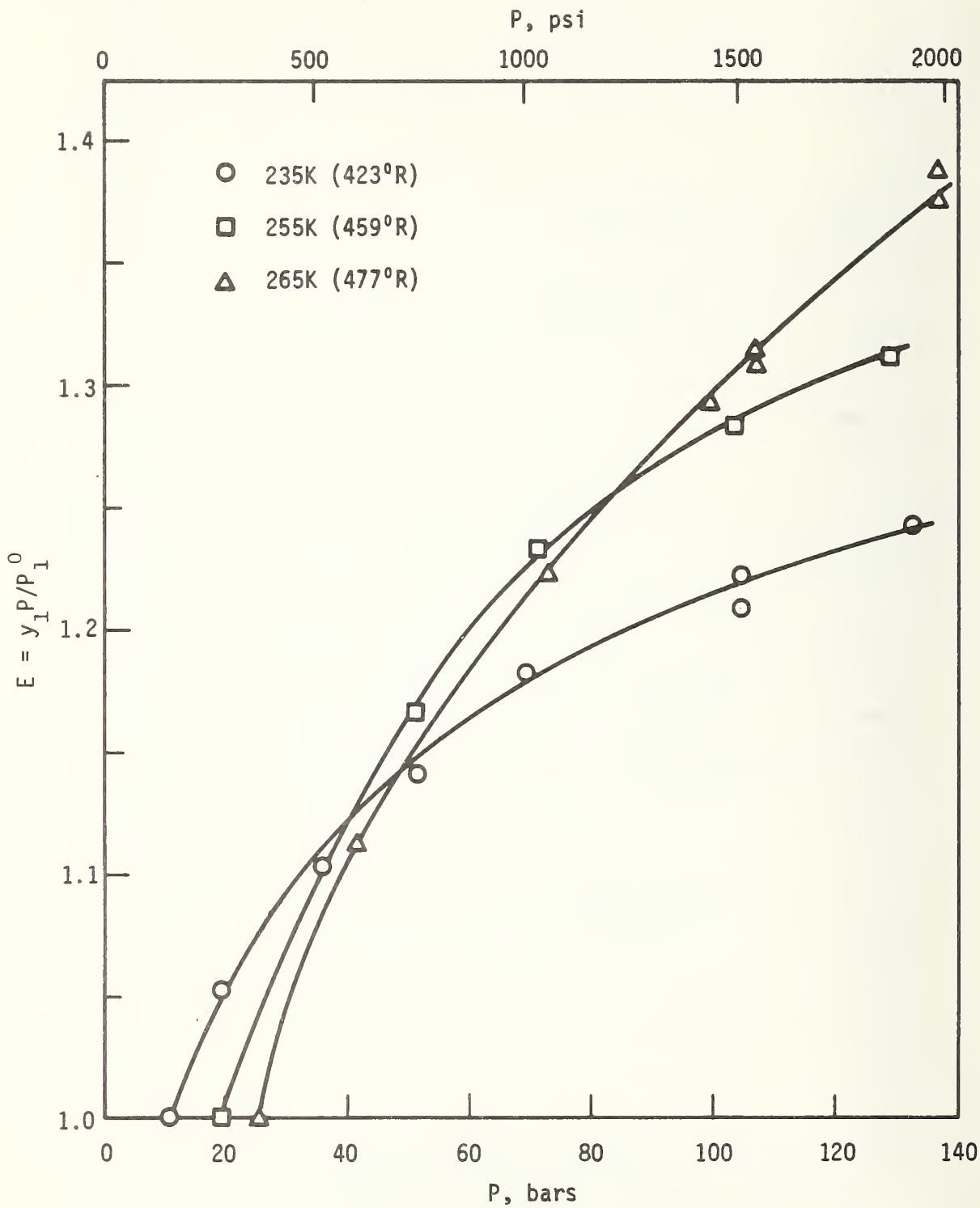


Figure 7. Enhancement factor for the He-N₂O system as a function of pressure.

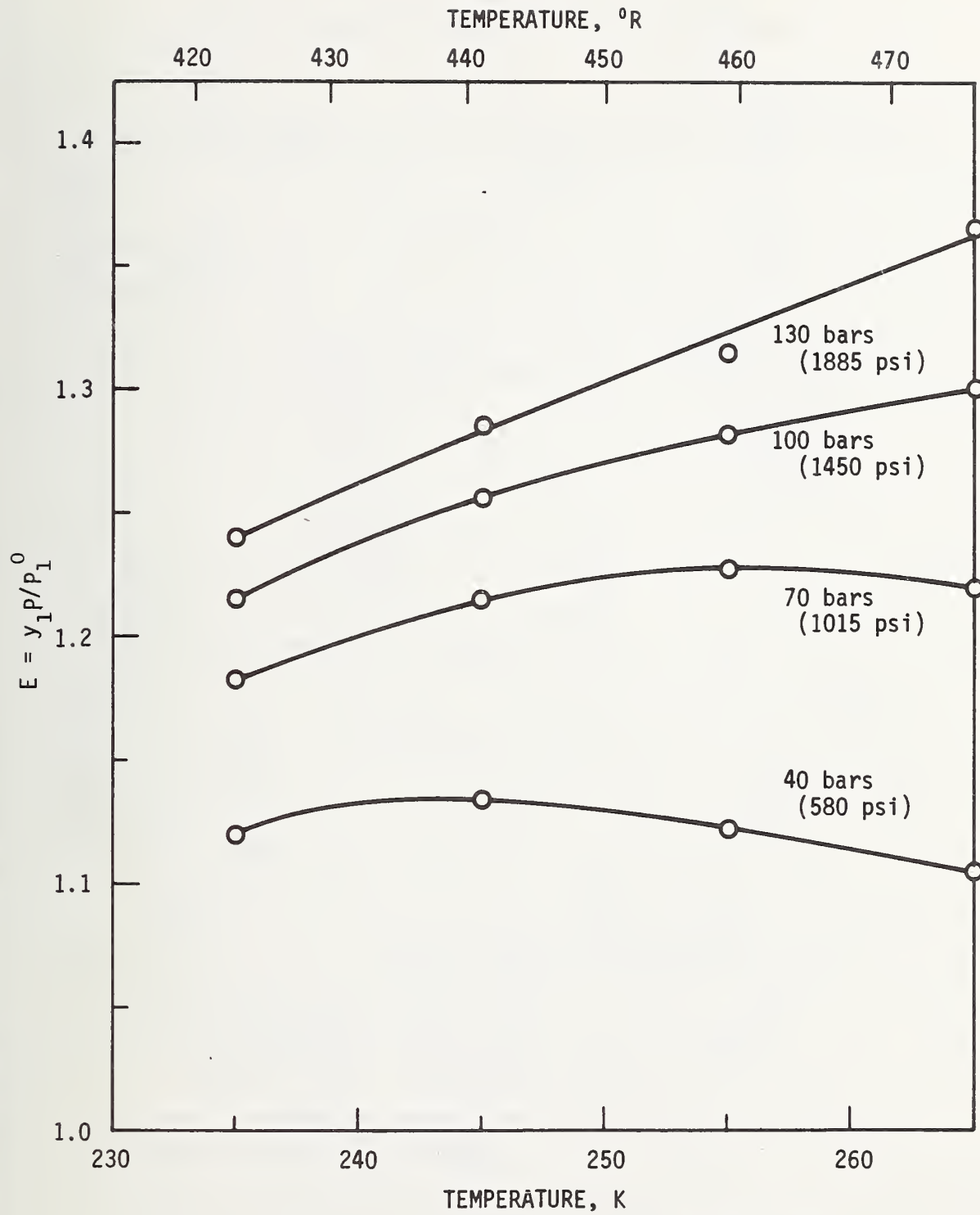


Figure 8. Enhancement factor for the He-N₂O system as a function of temperature.

3. Scale Model Flow-Induced Desorption Tests

3.1 Scaling Criteria

Figure 9 is a schematic showing the final configuration of the apparatus used at the National Bureau of Standards to measure the effect of helium desorption on flow rate. The apparatus models those features of the full scale systems which pertain to possible two-phase pipeline flow resistance and two-phase choking in a nozzle. Due to the temperature, pressure, and time dependence of gas solubility the essential characteristics of the full scale system to be duplicated in the model are the temperatures, pressure drops, and liquid residence times. A 6.7 m (22 ft.) length of 3.2 mm OD (1/8 in.) x 0.76 mm (0.030 in.) wall copper tubing provided the required pressure drop and residence time for the first series of liquid nitrogen tests. Table A1 in Appendix A shows the results of the first series of tests performed with liquid nitrogen. Runs 7 through 10 indicated that the effects of absorbed helium on flow were almost negligible in scaled long tubes. Consequently, we turned our attention to desorption effects in cavitating venturis (or flow control nozzles). The pressure drop in long tubes is gradual, but in nozzles it is quite rapid; therefore, the desorption potential and two-phase flow characteristics could be expected to differ. A venturi was installed along with a 91 cm (36 inch) length of 6.35 mm OD (1/4 in.) x 1.24 mm (0.049 in.) wall tube to provide the proper residence time; the 6.7 m x 0.76 mm tube was removed and variable control of valve V5 provided the proper resistance. The purpose of this change was to allow pressure upstream from the venturi to be varied during a test. A second throttle valve (valve V23) was also added to permit adjustment of the pressure downstream from the venturi.

To expedite the testing, the model supply and receiver reservoirs were sized to be compatible with existing dewars, catch tank, and plant facilities, and to give reasonable run times. The volume of the supply and receiver reservoirs is 0.303 ℓ (0.107 ft³).

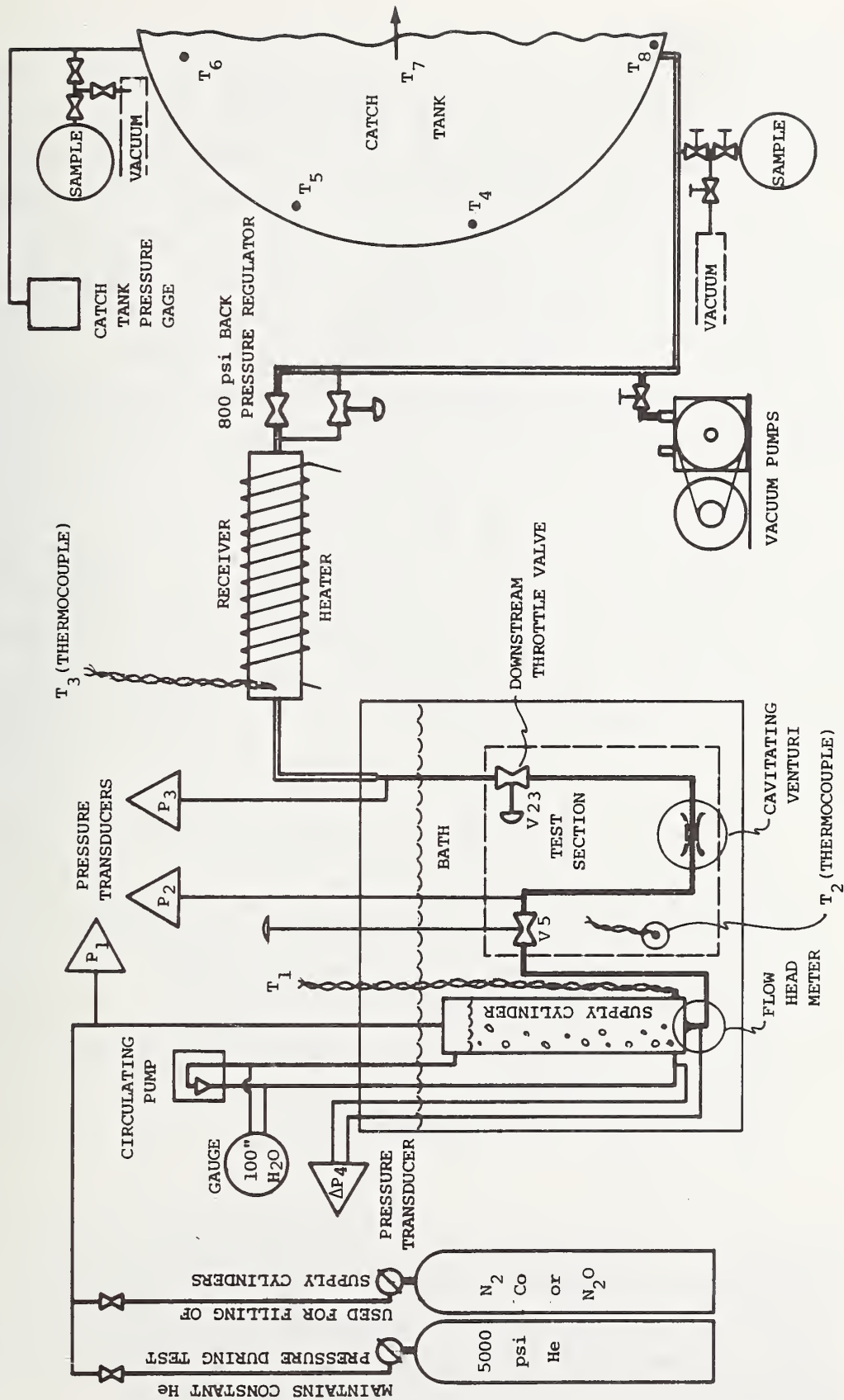


Figure 9. Flow induced desorption test apparatus. Configuration used in final tests (see Appendix A2).

3.2 Instrumentation

Temperatures at the bottom of the supply cylinder (T_1 in figure 9), in the stabilizing bath, T_2 , and in the receiver cylinder, T_3 , were sensed by Chromel-Alumel thermocouples and read out on a digital voltmeter. Pressure transducers-- P_1 at the supply inlet, P_2 at the restrictive tubing inlet, P_3 at the restrictive tubing outlet, and ΔP_4 , the flowmeter differential--were calibrated against secondary standard gauges before each test run. Pressures were recorded continuously during each test on a multichannel light beam galvanometer recorder.

The final pressure and temperature in the volume-calibrated catch tank (initially evacuated) determined the total mass of mixture transferred during the test. Pressure in the catch tank was measured with a quartz bourdon tube pressure gauge of 0-1000 mm Hg range, and temperature was measured with mercury thermometers in the catch tank. The instantaneous flowrate was indicated by a head meter at the discharge of the supply cylinder. The meter was calibrated by comparison with the catch tank integrated mass flow for several steady state runs of known duration (see sec. 3.4.1). The overall uncertainty of test measurements is as follows:

1. Temperature (thermocouples) -- $\pm 1.0^\circ\text{R}$ (± 0.6 K)
2. Mass flow rate (head meter) -- $\pm 1.5\%$ variation about stated C_d for CO, N_2 , and N_2O
3. Pressure (transducers) -- $\pm 2.0\%$ of the lowest readings for P_1 , P_2 , and P_3 (better for higher readings)
4. Pressure (quartz bourdon tube) -- ± 0.45 mm Hg
5. Flow meter differential pressure (transducer) -- $\pm 1.5\%$ of lowest readings for ΔP
6. Composition analysis -- ± 0.05 mole %.

3.3 Test Procedure

The supply cylinder was filled with liquid by simply condensing the appropriate gas. Bath temperature was maintained by 1) controlling the liquid nitrogen bath pressure for CO and N_2 test fluids, and 2) circulating chilled ethylene glycol for N_2O test fluid. Bath temperature control was maintained within ± 0.6 K for all experiments.

Flow tests were carried out with liquid nitrogen, liquid carbon monoxide, and liquid nitrous oxide. To establish the effects of dissolved helium, each test under a given set of flow conditions was performed with the supply liquid unsaturated and then saturated with helium gas. Saturation was accomplished by recirculating helium gas by means of a small magnetically driven pump shown in figure 9. The helium gas was introduced at the bottom of the supply cylinder and allowed to bubble up through the liquid for approximately forty-five minutes before each test with saturated fluid. The degree of saturation was verified after each test by mass spectrometer analysis of gas samples taken from the catch tank. For unsaturated test runs the absorption of helium was kept to a minimum by pressurizing at the top of the supply cylinder and starting the run immediately. Further preparation for a test run consisted of calibrating the pressure transducers, evacuating the catch tank, purging the downstream tubing, and pressurizing the receiver to the required back pressure. The purpose of this pre-pressurization was to minimize the time needed to establish steady flow. The purpose of the receiver cylinder is to maintain a constant back pressure during the flow desorption tests. Heating of the receiver cylinder prevented two-phase flow through the back pressure regulator and minimized the mass of residual fluid remaining in the receiver cylinder following a test.

Each test was started by opening valve V5. In some cases a steady flow was maintained throughout the entire test consuming most of the volume of the supply cylinder. In other "burst tests" the flow was maintained only long enough to establish steady flow conditions. Operating parameters such as upstream or downstream valve positions could then be changed and another test made without refilling the supply cylinder. In this way a series of runs were made in rapid succession. Repetitive tests were performed to verify the consistency of these data.

3.4 Results and Discussion

Early test results (before run 41) are slightly inconsistent showing the consequences of undeveloped procedures. Also, lower saturation pressures were specified by the sponsor for succeeding tests. The early test results are tabulated for completeness in the first part of Appendix A (Table A1); however, they have not been plotted or processed further.

Instrumentation precision, calibration, and test procedures were revised, and lower saturation pressures were used after run 41. Only these later results are discussed in this section and the data are tabulated in Table A2.

3.4.1 Head Meter Flow Coefficient

A converging nozzle leading from the supply cylinder to the test section inlet tubing served as the primary element of a flow head meter. The square root of the pressure differential between the supply cylinder and the flow nozzle throat, $\sqrt{\Delta P_4}$, is proportional to the mass flow rate \dot{W} . In the analysis of the data in this report $\sqrt{\Delta P_4}$ is used rather than \dot{W} ; however, a means of determining \dot{W} from tabulated values of ΔP_4 in Appendix A is given in this section for future reference. The flow meter was calibrated by means of seven steady state nitrogen runs and four nitrous oxide runs. To facilitate the determination of mass flow rate from values of ΔP_4 for all three fluids, a discharge coefficient, C_d , has been calculated. In this case the discharge coefficient has been defined in the most useful, simplified form as

$$C_d = \dot{W} / \sqrt{\Delta P_4 \rho_\ell}. \quad (3.1)$$

The discharge coefficient is a function of the Reynolds number which, for a given flow meter, is proportional to \dot{W}/μ_ℓ .

The values of C_d for N_2 as calculated from (3.1) were corrected upward by 0.8% for the flow meter throat cross sectional area reduction due to the lower temperature of N_2 . Over the range of \dot{W}/μ_ℓ covered in these experiments C_d was repeatable for each fluid to within 1.5% of the average value. However, the average value differed for the two fluids as follows:

$$\bar{C}_d = 20.5 \frac{\text{g}}{\text{s}} / \sqrt{\text{bars} \cdot \frac{\text{g}}{\text{cm}^3}} \quad (= 1.55(10)^{-3} \frac{\text{lb}}{\text{s}} / \sqrt{\frac{\text{lb}}{\text{in}^2} \frac{\text{lb}}{\text{ft}^3}}) \text{ for } N_2, \text{ and}$$

$$\bar{C}_d = 22.0 \frac{\text{g}}{\text{s}} / \sqrt{\text{bars} \cdot \frac{\text{g}}{\text{cm}^3}} \quad (= 1.61(10)^{-3} \frac{\text{lb}}{\text{s}} / \sqrt{\frac{\text{lb}}{\text{in}^2} \frac{\text{lb}}{\text{ft}^3}}) \text{ for } N_2O.$$

It is believed that this discrepancy is due primarily to uncertainty in the density of the liquid N_2O . For this reason, and because of the similarity between N_2 and CO properties, it is recommended that the value of C_d obtained for N_2 be used for CO.

3.4.2 Resistive Flow

To analyze the worst case, it is assumed that helium gas is absorbed to the maximum (equilibrium) concentration under supply pressure and undergoes equilibrium desorption at the reduced pressure downstream in the system. Desorbed vapor volume and mass fraction of vapor were computed from the phase equilibrium data of section 2. Pressure drop due to two phase resistive flow was calculated by means of a correlation of Martinelli and Nelson [9]. An adaptation of this correlation was employed which is usable over the entire two phase range and reduces properly to single phase values for pure liquid or pure gas. The two-phase flow parameters used are shown in figure 10.

The pipeline axial pressure gradient is given by

$$\frac{dP}{dx'} = \theta \left[\frac{f_{tg} Y^{1.8}}{\rho_g} + \frac{f_{tl} (1 - Y)^{1.8}}{\rho_l} \right] \frac{G^2}{2D}, \text{ where the}$$

symbols are identified in the nomenclature of this paper.

The pressure gradient for a given flow is a function of the mass fraction of vapor which is, in turn, a function of the local pressure. The relationship of dP/dx to P is given in Figure 11 for a model He-N₂O flow rate per unit area of

$$G = 759 \frac{\text{g}}{\text{s} \cdot \text{cm}^2} \left(1556 \frac{\text{lb}}{\text{s} \cdot \text{ft}^2} \right)$$

and a supply liquid pressure,

$$P_1 = 75.8 \text{ bars (1100 psia)}.$$

Figure 11 shows that, in proceeding from high pressure pure liquid to lower pressures along the equilibrium two-phase flow curve, the pressure gradient does not rise steeply until the pressure falls below about 27.6 bars (400 psia). Pressure drop per unit length for the nearly incompressible unsaturated liquid flow varies little with

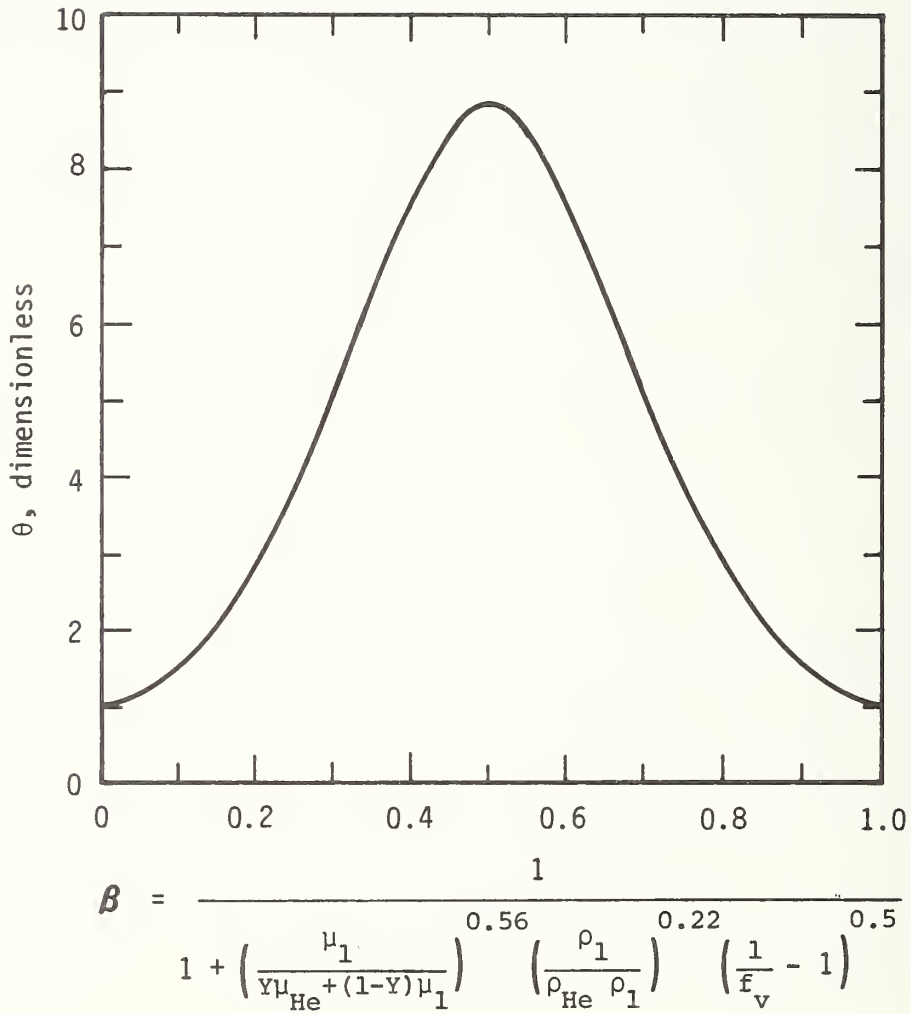


Figure 10. Adaptation of Martinelli and Nelson [9] correlation for two-phase flow resistance assuming no slip and both phases turbulent.

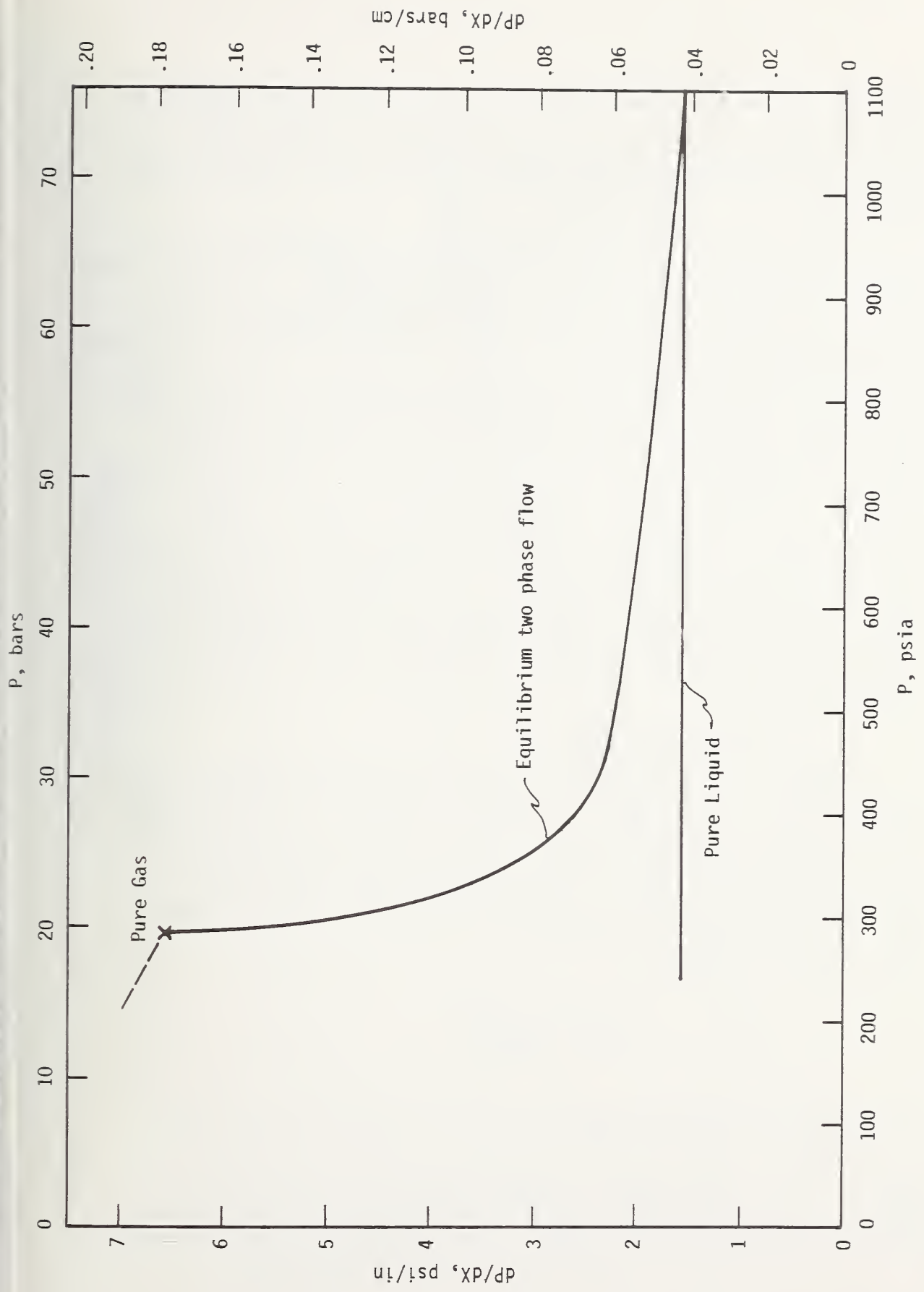


Figure 11. Axial pressure gradient as a function of local pressure for He-N₂O flow rate of 759 g/s-cm² (1555 lb/s-ft²) and initial pressure of 75.8 bars (1100 psia).

pressure. Since the minimum pressure, P_3 , in the resistive section did not fall below 44.8 bars (650 psia), one would not expect to see a difference between saturated and unsaturated liquids in these resistive flow experiments.

Figure 12, giving overall pressure drop by integration of the gradient, illustrates this point. To make the comparison it was necessary to use valve 5 stem position as an independent variable since that valve was the main resistive element and its setting varied. The ordinate of this curve is $(P_1 - P_2)/\Delta P_4$, which is proportional to $(P_1 - P_2)/W^2$, and amounts to a flow coefficient for the resistive plumbing. This coefficient should depend upon the valve position and two-phase frictional effects. The solid line is a smooth fit of all the unsaturated test data obtained in runs 54 and 55. With the solid line taken as a base, corresponding theoretical saturated liquid-equilibrium flow values were calculated and plotted as the dashed line. It is apparent that the largest estimated difference between the saturated flow and unsaturated flow curves is probably within experimental precision; this is born out by the experimental data.

3.4.3 Cavitating Venturi Flow

Pressures in the cavitating venturi are intended to drop to the vapor pressure at the throat. As shown in section 3.4.2 the two-phase flow resistive effects would become large at such low pressures if phase equilibrium prevailed. Even more restrictive would be the two-phase choking effect. For homogeneous, equilibrium flow the choking mass velocity is given by

$$G_{\max}^2 = \frac{C_u}{\left(-\frac{\partial v}{\partial P}\right)_s}$$

$(C_u = \text{a units conversion factor,}$

$\left(\frac{\partial v}{\partial P}\right)_s = \text{isentropic pressure derivative of mixture specific volume.})$

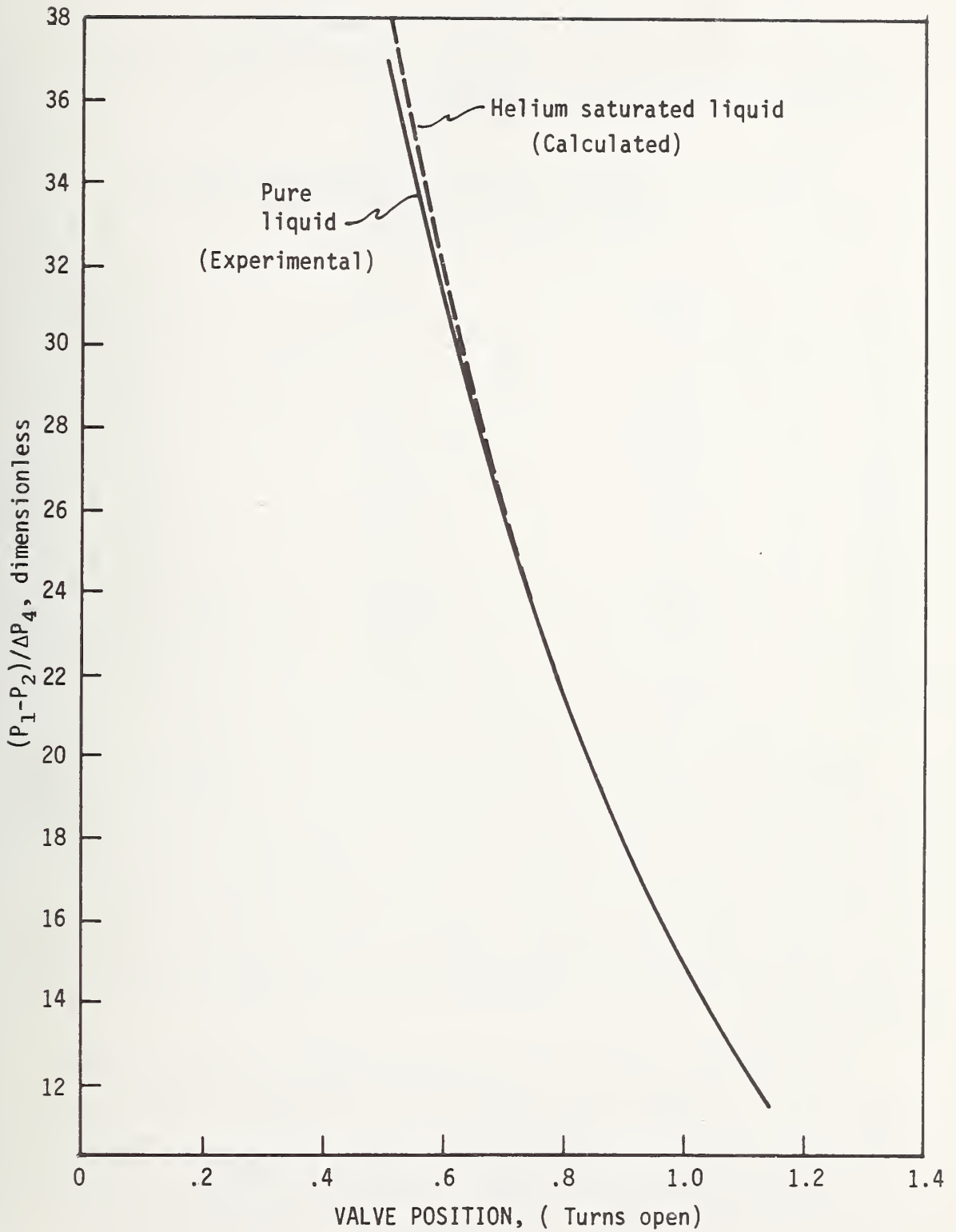


Figure 12. Over all pressure drop. Comparison between equilibrium flow of saturated N_2O and pure liquid.

Table 5 shows the relationship between G_{\max} and pressure computed from the He-N₂ phase equilibrium data for an initial pressure of 130 bars (1890 psia) and temperature of 77 K (138°R).

Table 5. Homogeneous equilibrium choking flow for He-N₂, initial pressure 130 bars (1890 psia), temperature 77 K (138°R).

P psia	P bars	G_{\max} lb/s · ft ²	G_{\max} g/s · cm ²
60	4.14	670	327
100	6.89	3,400	1,660
200	13.8	11,500	5,610
300	20.7	19,000	9,280
500	34.5	32,000	15,600
800	55.2	50,000	24,400
1000	68.9	60,000	29,300
1500	103.4	84,000	41,000
1890	130.3	103,000	50,300

Experimental saturated nitrogen flow under these initial conditions reached 21.8 g/s (0.048 lb/s), which results in $G = 15,600 \text{ g/s} \cdot \text{cm}^2$ (32,000 lb/s · ft²) in the venturi throat. Bernoulli's equation predicts 1.38 bars (20 psia) at the throat for pure liquid flow at this flow rate, whereas table 5 shows that $G_{\max} < 670 \text{ lb/s} \cdot \text{ft}^2$ at 20 psia, or one fiftieth of the actual mass velocity. This calculation merely shows that the phase equilibrium assumption results in a gross miscalculation of venturi flow.

The experimental data for all three fluids do indicate a small effect of flow-induced helium desorption in the venturi, however. In figures 13-17 the $\sqrt{\Delta P_4}$ -- which, except for a constant, is equivalent to W -- is plotted against P_2 , the venturi upstream pressure. The maximum reduction in flowrate due to helium saturation is shown in table 6.

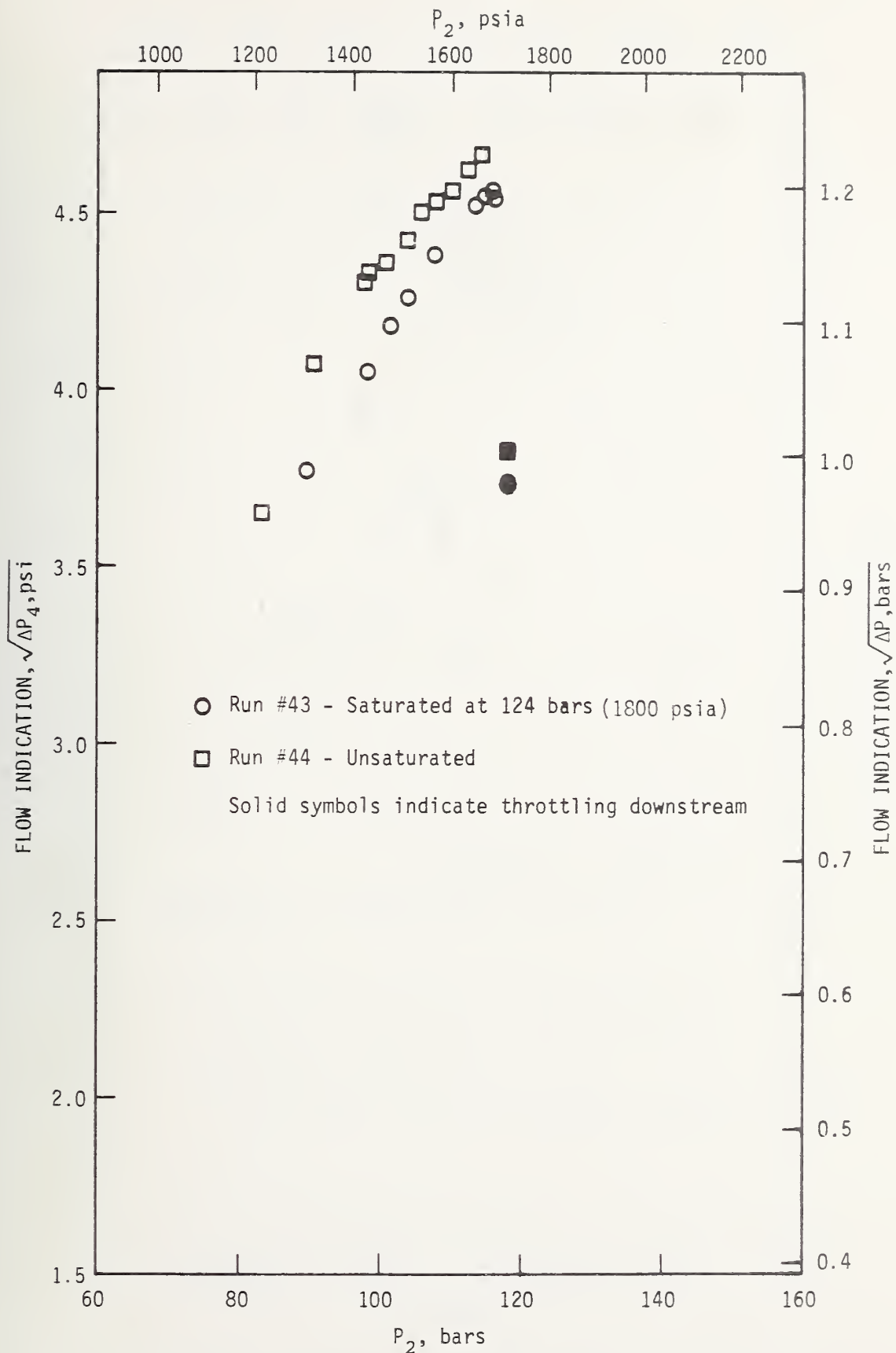


Figure 13. Flow rate indication as a function of nozzle upstream pressure for liquid nitrogen at 80.3K (145°R).

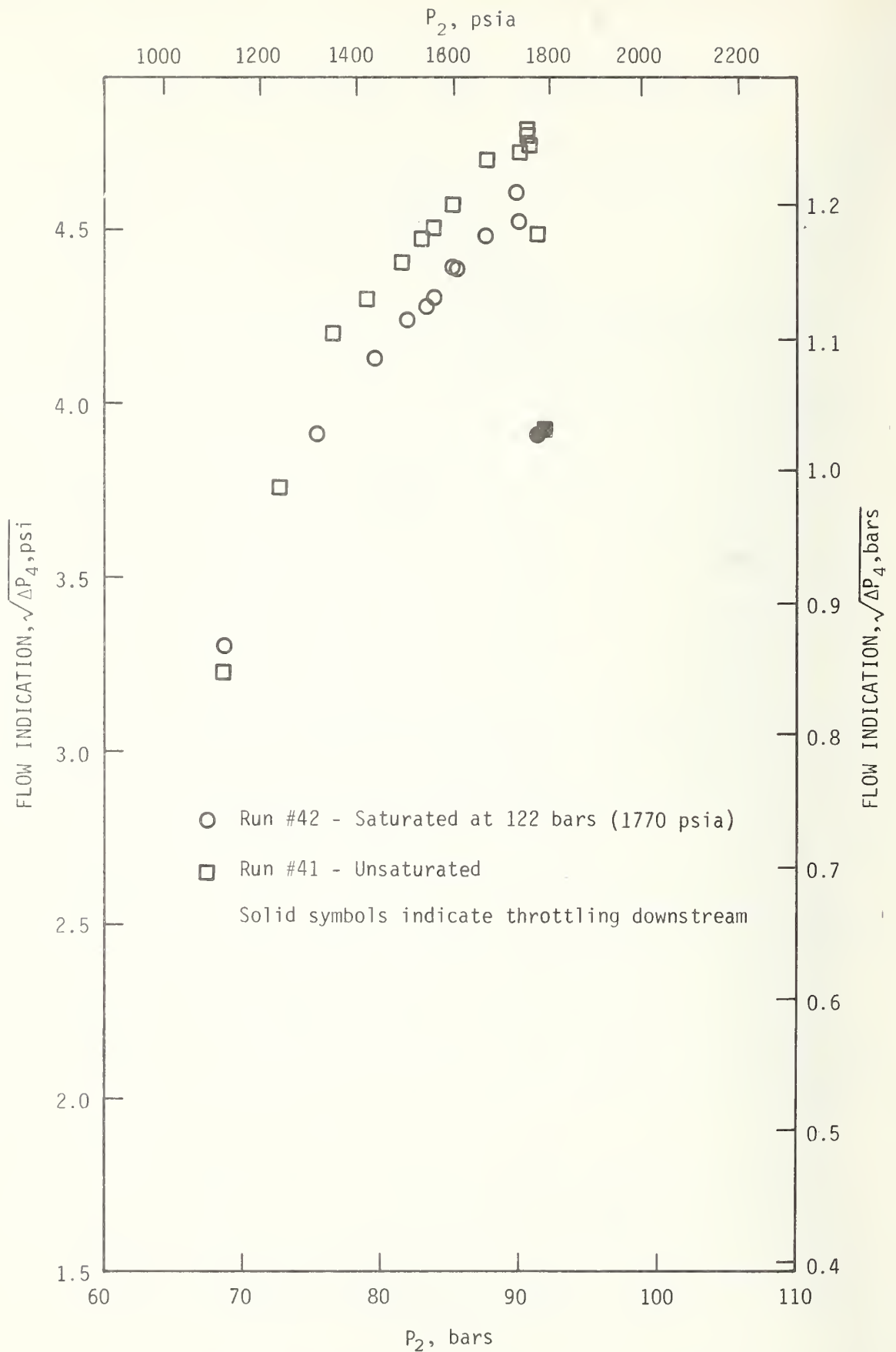


Figure 14. Flow rate indication as a function of nozzle upstream pressure for liquid carbon monoxide at 85.3K (153°R).

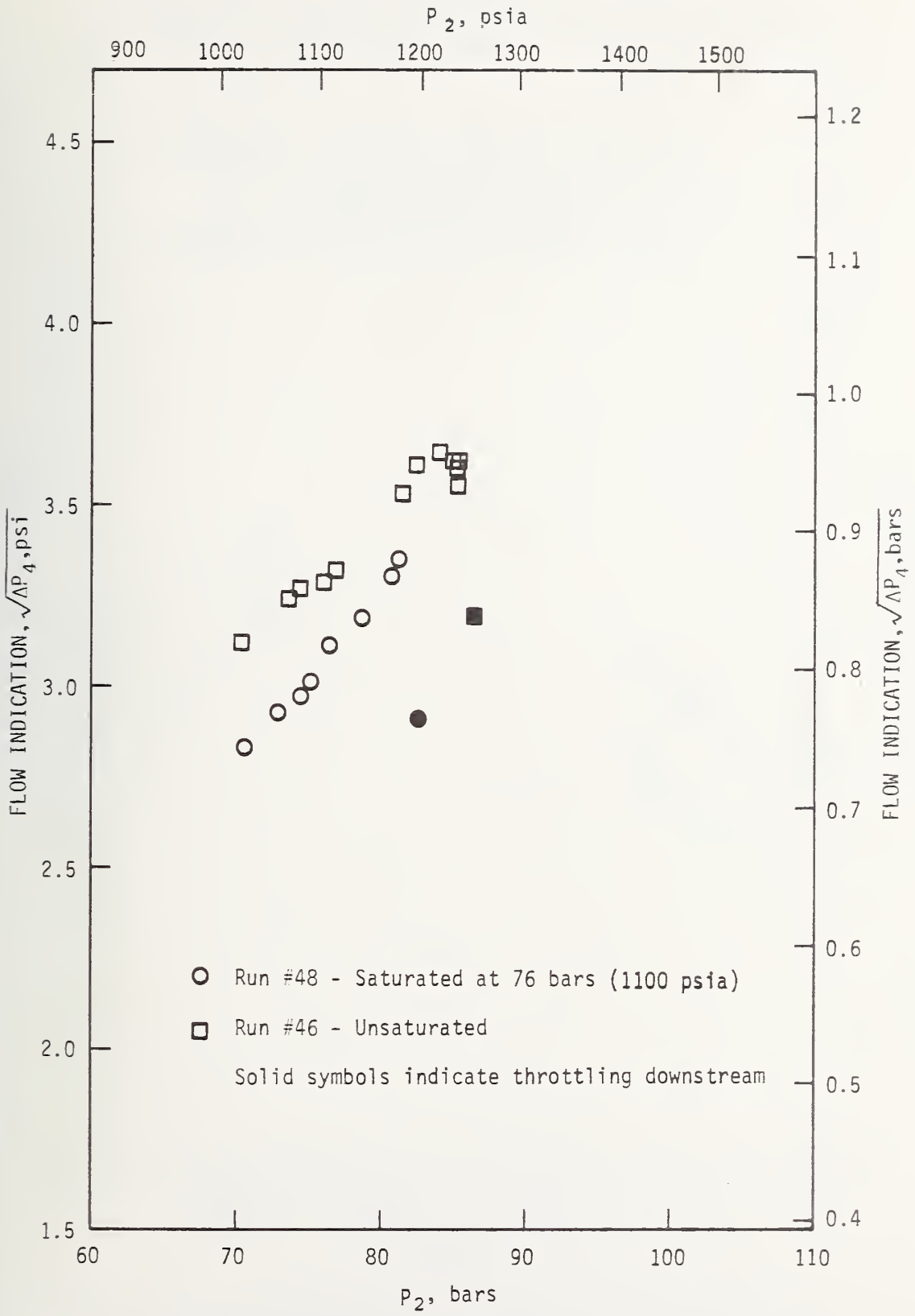


Figure 15. Flow rate indication as a function of nozzle upstream pressure for liquid nitrous oxide at 255K (459°R).

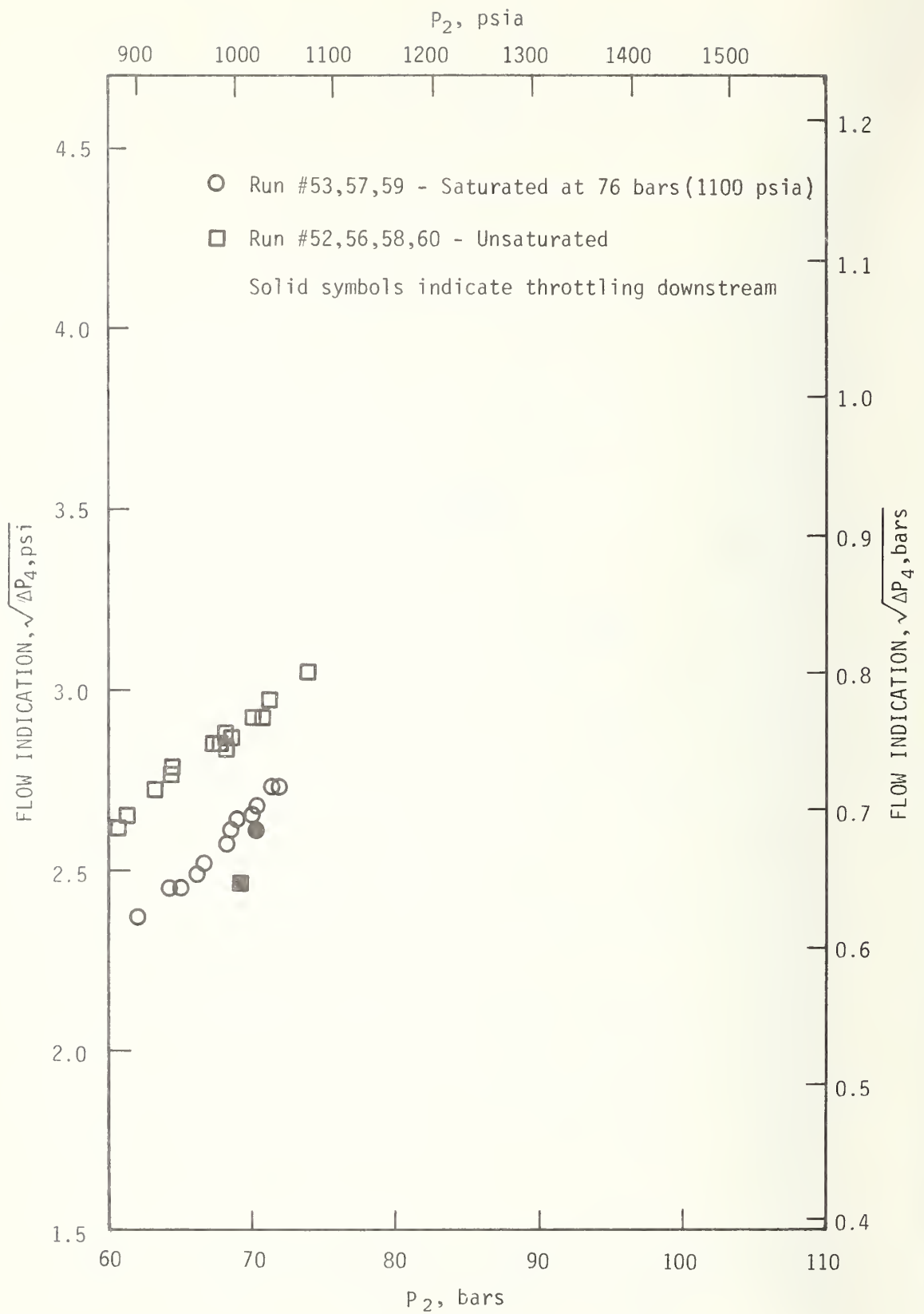


Figure 16. Flow rate indication as a function of nozzle upstream pressure for liquid nitrous oxide at 266K (479°R).

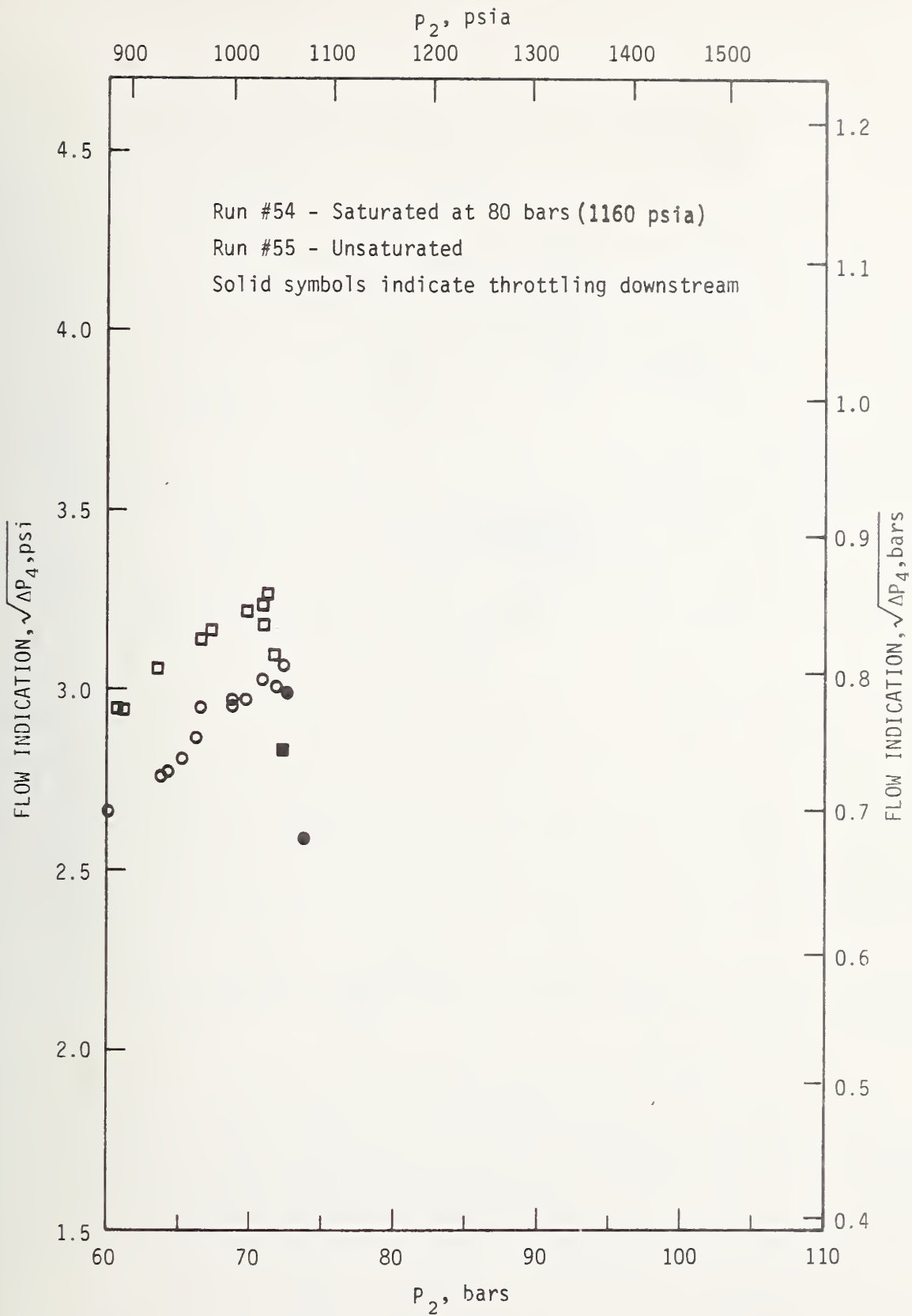


Figure 17. Flow rate indication as a function of nozzle upstream pressure for liquid nitrous oxide at 244K (439°R).

Table 6. Reduction of flow rate due to helium saturation.

Fluid	Runs No.	Nominal		Maximum Flow Rate Reduction, %
		$^{\circ}\text{R}$	T_{sat} K	
N_2	43,44	144	80.2	4
CO	41,42	153	85.3	4
N_2O	46,48	459	255.	9
N_2O	52,53,56-60	480	266.	12
N_2O	54,55	439	244.	9

Experimental data points involving cavitation can best be distinguished from noncavitating data points in figures 18-22. The rationale behind the coordinates used in these figures is as follows:

Non-cavitating flowrate through the venturi is approximately proportional to the square root of the pressure drop across the venturi,

$$\dot{W} \propto \sqrt{P_2 - P_3},$$

and for the flow meter,

$$\dot{W} \propto \sqrt{\Delta P_4}.$$

In non-cavitating flow a reduction in the pressure P_3 downstream from the venturi (by opening valve V23) increases $\sqrt{P_2 - P_3}$, increases the flowrate, and correspondingly increases $\sqrt{\Delta P_4}$. Normalization of the quantities $\sqrt{P_2 - P_3}$ and $\sqrt{\Delta P_4}$ by dividing each of them by $\sqrt{P_2 - P_{\text{sat}}}$ does not change this trend; i.e., for non-cavitating flow an increase in $\sqrt{\frac{P_2 - P_3}{P_2 - P_{\text{sat}}}}$ is accompanied by an increase in $\sqrt{\frac{\Delta P_4}{P_2 - P_{\text{sat}}}}$.

When the flow through the venturi is initially non-cavitating a reduction in P_3 reduces the pressure in the venturi throat until cavitation begins. In the case of a neat fluid cavitation occurs at or slightly below the vapor pressure, and in a helium saturated fluid cavitation may begin when the helium gas begins to desorb. A further reduction in P_3 does not correspondingly increase the flowrate, but rather increases the extent of cavitation while the venturi throat pressure remains near P_{sat} or a slightly higher desorption pressure. In this cavitating condition the flowrate is affected very little by changes in P_3 and the flowrate is

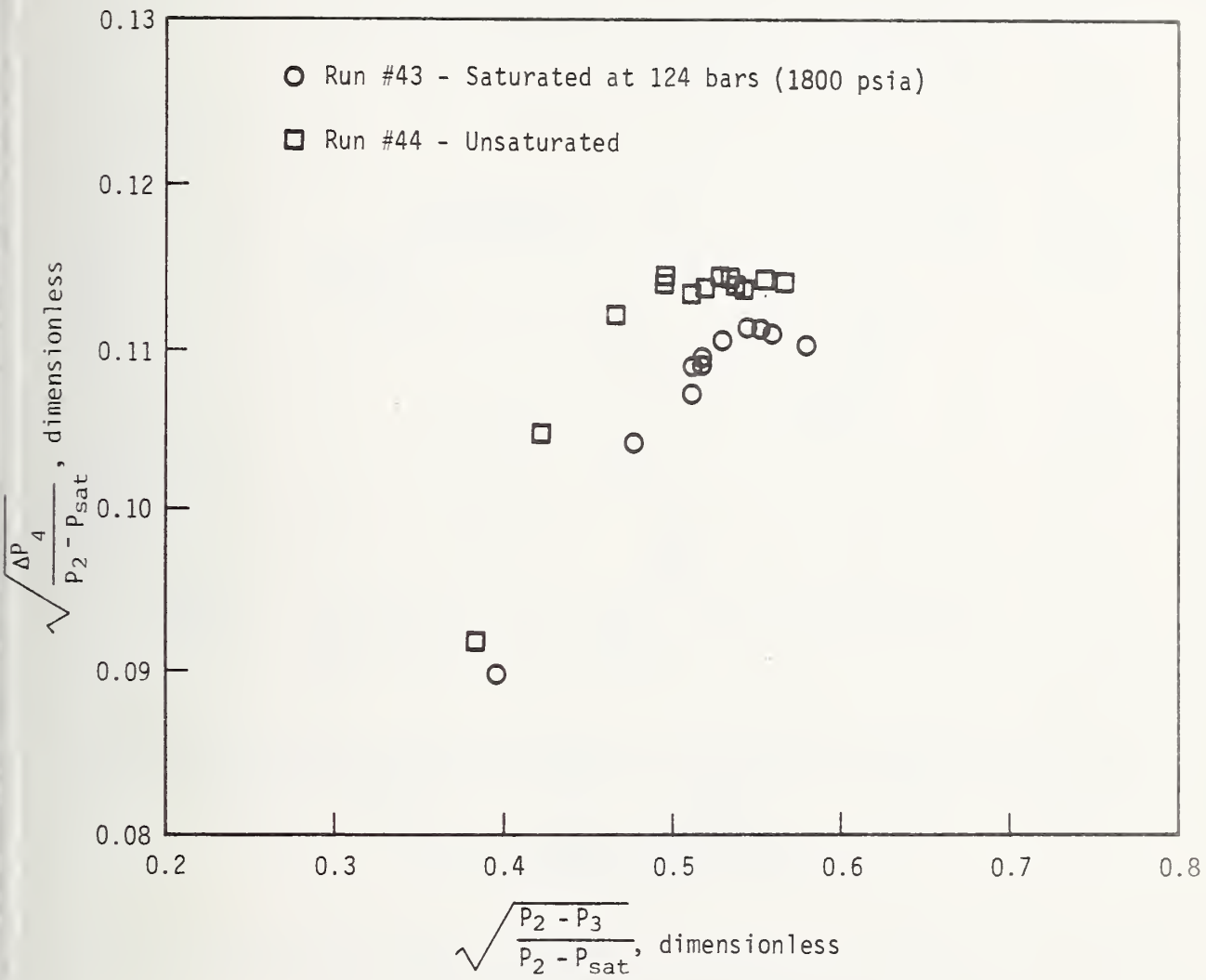


Figure 18. Cavitation parameter as a function of nozzle pressure drop parameter for liquid nitrogen at 80.3K (145°R).

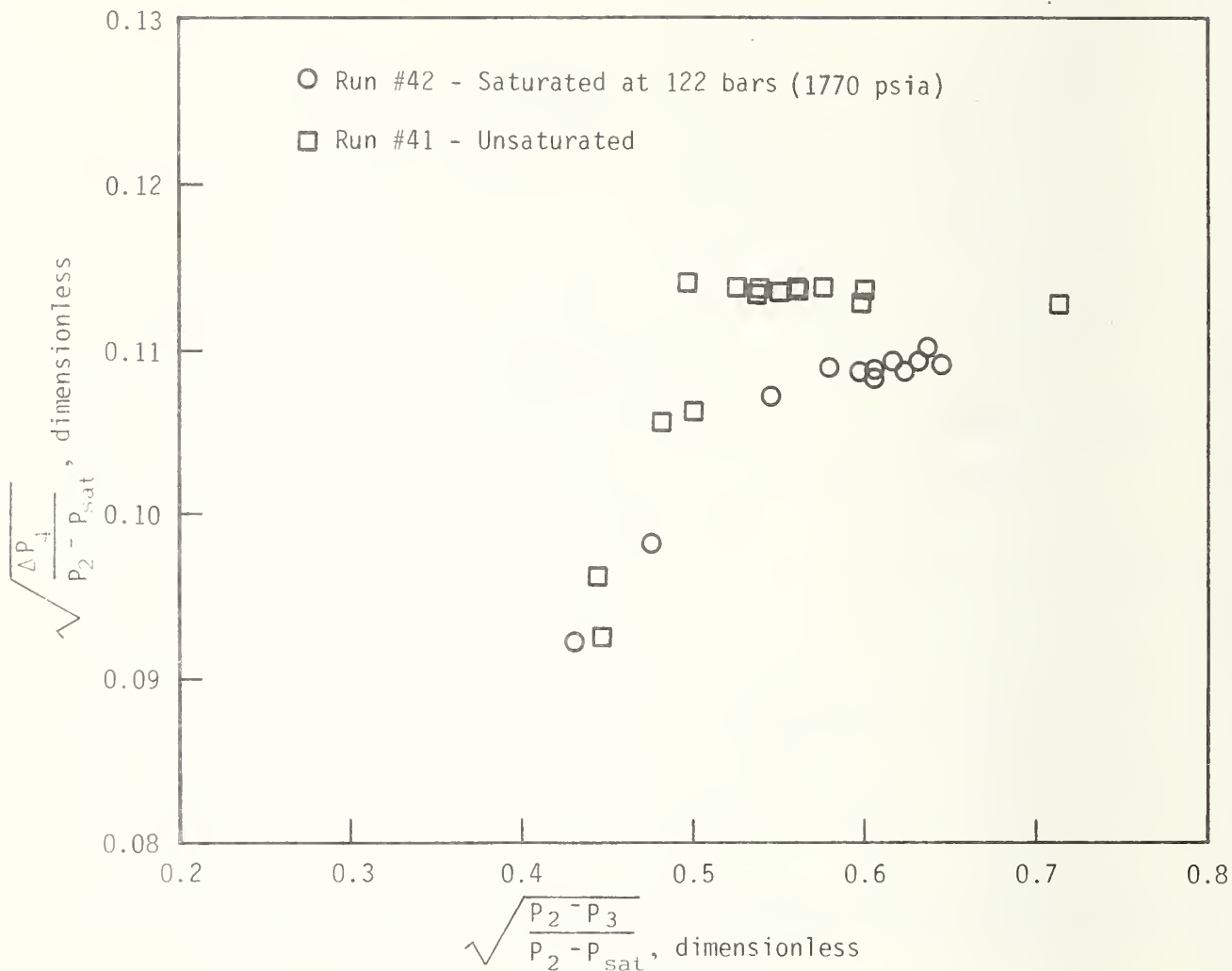


Figure 19. Cavitation parameter as a function of nozzle pressure drop parameter for liquid carbon monoxide at 85.3K (153°R).

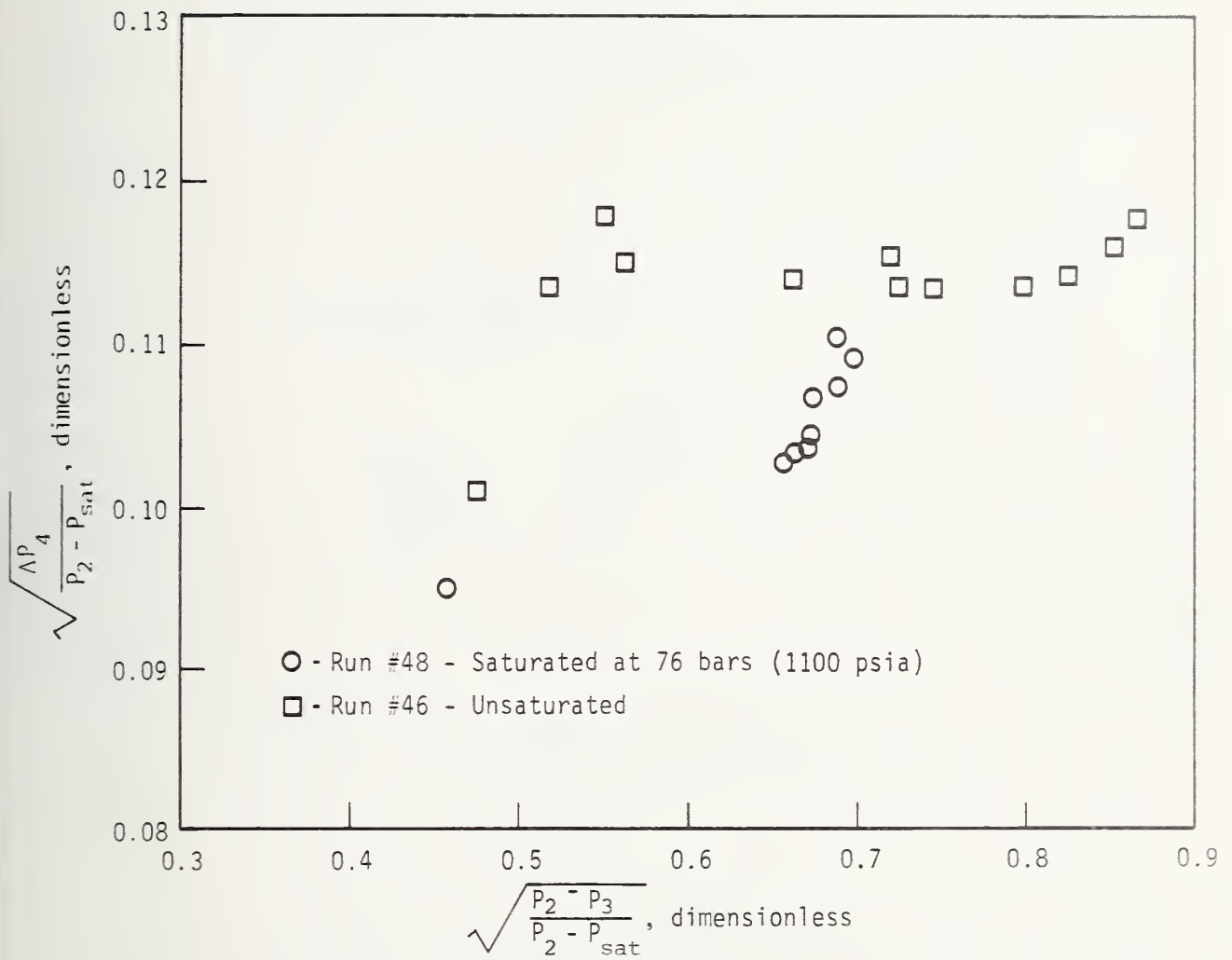


Figure 20. Cavitation parameter as a function of nozzle pressure drop parameter for liquid nitrous oxide at 255K (459°R).

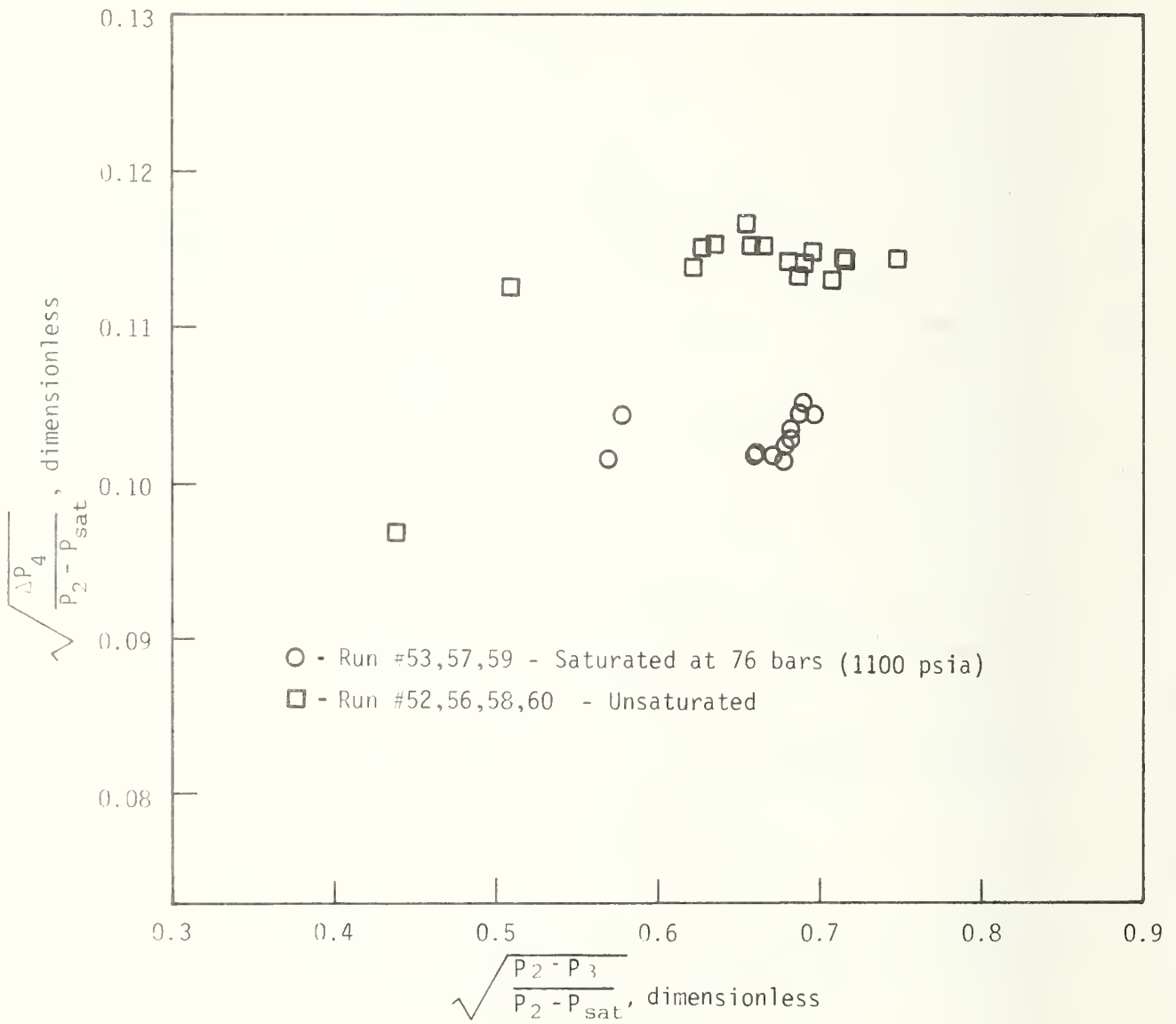


Figure 21. Cavitation parameter as a function of nozzle pressure drop parameter for liquid nitrous oxide at 266K (479°R).

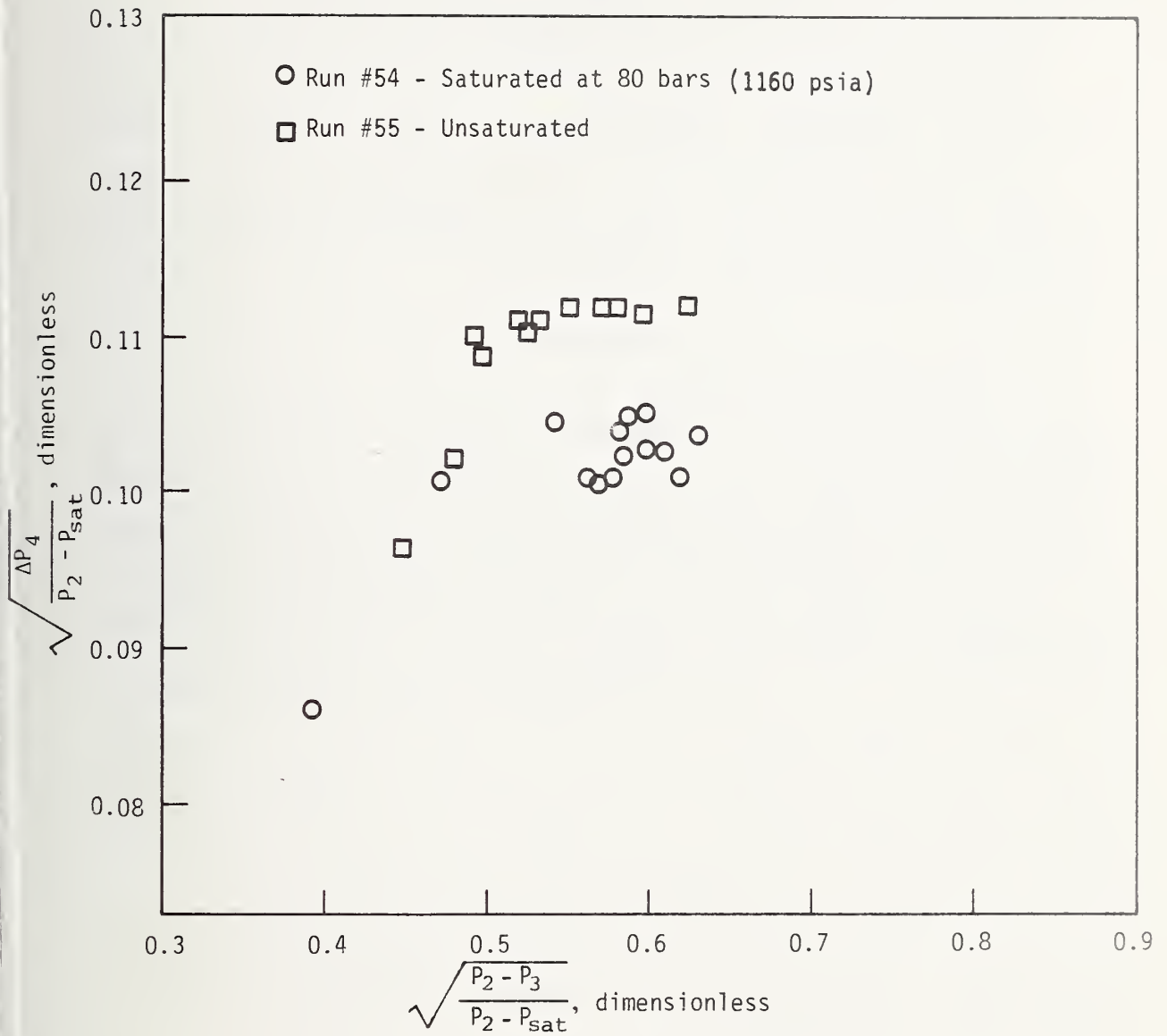


Figure 22. Cavitation parameter as a function of nozzle pressure drop parameter for liquid nitrous oxide at 244K (439°R).

approximately, $W \propto \sqrt{P_2 - P_{\text{sat}}}$; therefore while the quantity $\sqrt{\frac{\Delta P_4}{P_2 - P_{\text{sat}}}}$ is relatively constant, the quantity $\sqrt{\frac{P_2 - P_3}{P_2 - P_{\text{sat}}}}$ may vary widely.

The onset of cavitation may then be identified in figures 18-22 as the region in which $\sqrt{\frac{\Delta P_4}{P_2 - P_{\text{sat}}}}$ becomes relatively flat. The effect of helium saturation in reducing slightly the flowrate $\left(\sqrt{\frac{\Delta P_4}{P_2 - P_{\text{sat}}}}\right)$ at which cavitation occurs may also be seen in figures 18-22.

3.5 Experimental Observations

Two phenomena observed during the testing of the CO and N₂O systems are noteworthy: (1) CO pressure oscillations in the transmitting tubes leading to the pressure transducers, and (2) the formation of slush when the N₂O system was vented rapidly. The oscillations were eliminated without significantly affecting the pressure response time by inserting wires into the instrument lines for frictional damping, and by adding a small expansion volume in the transmitting tubing. The latter was located adjacent to the transducer and sized to eliminate oscillations. The mixture of liquid-solid N₂O (slush N₂O) formed when the system was vented rapidly because Boulder, Colorado atmospheric pressure is below the N₂O triple point pressure. It is important to note this occurrence since it pertains to the possible venting of N₂O systems in subatmospheric environments. Such formation of slush or solid may cause partial or total bleed line blockage, flow disruptions, and inability to drain the N₂O tank. Gradual venting and/or addition of heat during venting prevents this slush formation.

4. Conclusions

Liquid and vapor phase compositions have been measured for the helium-carbon monoxide system between 80 and 120 K and for the helium-nitrous oxide system between 235 and 285 K. Using enhancement factors and Henry's Law constants as a guide, the data for each phase appear internally consistent and have the proper qualitative behavior.

The effects of helium absorption and flow induced desorption were investigated by means of scale model experiments. Calculations by a two phase flow correlation, using the phase equilibrium data of this study, indicate that the flow resistance effect of desorbed helium in long pipelines would be almost negligible until the pressure in the system dropped below about 27 bars (400 psia). Since this calculation was based on the worst case of assumed phase equilibrium the resistive effects in the actual flow stream, in which the pressure dropped no lower than 46 bars (675 psia), were expected to be even less. The experimental data verified this calculation and reasoning and showed no appreciable two-phase resistive effects. Contrarily, phase equilibrium calculations for the flow nozzle indicated that two phase choking would occur at extremely low flow rates with helium saturated liquids. However, actual experimental flow rates were fifty times as great as the calculated equilibrium choking flow rates. A definite effect of helium desorption was detected in the nozzle flow tests; though smaller than theoretical, this effect ranged from a four percent flow reduction for N_2 and CO to a twelve percent reduction in N_2O . From these data we may conclude that the assumption of phase equilibrium in a flow nozzle or venturi leads to gross miscalculations.

5. References

1. Sinor, J. E. and Kurata, F., J. Chem. Eng. Data 11, 537 (1966).
2. Kling, G., Chem. Ingr. Tech. 38, 1080 (1966).
3. Duncan, A. G. and Hiza, M. J., Advances in Cryogenic Engineering, Edited by K. D. Timmerhaus, 15, 42, (Plenum Press, New York, N.Y. 1970).
4. Wagner, W., Cryogenics 13, 470 (1973).
5. Lewis, G., Pratt Whitney Aircraft, West Palm Beach, Fla., private communication, (1973).
6. Hust, J. G. and Stewart, R. B., Nat. Bur. Stand. (U.S.) Tech. Note No. 202, (1963).
7. Buzyna, G., Macries, R. A. and Ellington, R. T., Chem. Eng. Progr. Symp. Ser. 59 (44), 101 (1963).
8. Hiza, M. J. and Duncan, A. G., Advances in Cryogenic Engineering Edited by K. D. Timmerhaus, 14, 30, (Plenum Press, New York, N.Y., 1969).
9. Martinelli, R. C. and Nelson, D. B., ASME Transactions 70: 695-716 (1948).

Appendix A1

The objective of runs 7 to 10 was to determine the effect (if any) of desorbed helium gas on the flow resistance in a 6 m (22 ft) length of 1.65 mm (0.065 in) ID tubing.

The venturi was first installed for runs beginning with no. 16. The objective of runs 16 through 40 was to determine the downstream pressure (varied by valve V23 setting) at the transition between non-cavitating and cavitating venturi flow. In runs 34 to 40 a 0.61 mm (0.024 in) throttling orifice was installed upstream of V5 to provide the desired pressure drop. A 91 cm (36 inch) length of 6.35 mm (1/4 in) OD x 1.24 mm (0.049 in) wall tubing provided the required residence time and replaced the 22 ft tube used in tests 7 to 33. Several of the tests in Table A1 (starting with run 15) were "burst tests" in which valve V23 was varied during the test while all other test parameters were held constant. The objective of these tests was to investigate the effects (on flow) of varying pressure downstream of the venturi for neat and helium-saturated fluids.

Table A1. Early test results - Nitrogen.

Run #	Saturated	Unsaturated	P ₁ atm	P ₂ atm	P ₃ atm	ΔP ₄ psi	P _{sat} atm	T K	Helium Saturation Pressure atm	V5 Position (turns open)	V23 Position (turns open)
7		X	117.5	108.3	52.0	18.2	0	75.9	--	w.o.*	**
8†	X		123.2	111.5	52.5	18.9	0	75.9	128	w.o.	**
9†		X	120.	111.0	54.0	19.7	0	75.8	--	w.o.	**
10†	X		139.	120.0	55.0	21.2	0	75.9	128	w.o.	**
16†		X	128.	118.	94	15.6	0	75.9	--	w.o.	3-1/2
17†	X		130.	118.	94	15.6	0	75.9	127.5	w.o.	3-1/2
18†		X	128.5	113	81	21.0	0	75.9	--	w.o.	5
19	X		135	117	82	21.4	0	75.9	127.5	w.o.	5
15		X	128	117.5	60	19.2	0	75.9	N/A	w.o.	14
15	X		129	118	60	19.4	0	75.9	N/A	w.o.	13
15	X		129	118	62	19.4	0	75.9	N/A	w.o.	11
15	X		130	119	66	19.4	0	75.9	N/A	w.o.	9
15	X		130	120	68	19.6	0	75.9	N/A	w.o.	8
15	X		130	121	84	19.8	0	75.9	N/A	w.o.	5
15	X		132	123.2	93.3	18.4	0	75.9	N/A	w.o.	4
15	X		132	124	96	16.0	0	75.9	N/A	w.o.	3-1/2
15	X		131	124	99	14.4	0	75.9	N/A	w.o.	3
20	X		128	112.5	69	20.4	0	75.9	127.5	w.o.	8
20	X		129	114	82	20.9	0	75.9	127.5	w.o.	5
20	X		128	113	89.5	19.2	0	75.9	127.5	w.o.	4
20	X		129	116.5	93.2	16.2	0	75.9	127.5	w.o.	3-1/2
20	X		128	115	95.0	15.0	0	75.9	127.5	w.o.	3

† Indications of slight plugging in flowmeter; paired comparisons of (9&10), (16&17) OK

Nozzle blockage occurred also

* wide open

** valve V23 not installed at this time- a long tube(6.7m x 0.76mm ID) provided most of the flow resistance

all pressures are gage atm

Table A1. Early test results - Carbon Monoxide.

Run #	Saturated	Unsaturated	P ₁ atm	P ₂ atm	P ₃ atm	ΔP ₄ psi	P _{sat} atm	T K	Helium		V23 Position (turns open)
									Saturation Pressure atm	V5 Position (turns open)	
36	X		203	124	98	21.1	0.660	85.22	196	w.o.	3-1/2
36	X		202	120.5	84.5	21.7	0.660	85.22	196	w.o.	4-1/2
36	X		202	120	75.8	21.7	0.660	85.22	196	w.o.	5-1/2
36	X		202	121	75.8	21.8	0.660	85.22	196	w.o.	5-1/2
36	X		201.7	120	70.2	21.7	0.660	85.22	196	w.o.	6-1/2
25		X	196.4	112.2	90.2	14.42	-0.314	76.17	--	w.o.	3-1/2
29		X	190	97.3	72.5	16	-0.314	76.17	--	w.o.	5-1/2
26	X		203	115	93.4	16.3	-0.314	76.17	196	w.o.	3-1/2
30	X		193.2	95.5	72.2	15.8	-0.314	76.17	196	w.o.	5-1/2
33	X		199	87	66.5	15.60	-0.382	76.18	196	w.o.	6-1/4
33	X		199	93	71.5	15.80	-0.382	76.18	196	w.o.	5-1/2
33	X		199	107.8	84.2	16.60	-0.382	76.18	196	w.o.	4-1/4
33	X		199	147.7	128.8	14.00	-0.382	76.18	196	w.o.	2-1/2
33	X		200	127.6	104.5	17.80	-0.382	76.18	196	w.o.	3-1/2
33	X		201.2	142.6	121.5	17.40	-0.382	76.18	196	w.o.	3
ORIFICE INSTALLED upstream of V-5 FOLLOWING # 33											
37	X		200	133.3	106.5	18.7	0.662	85.27	196	w.o.	3
37	X		200	132.7	106	18.8	0.662	85.27	196	w.o.	3
37	X		200	124	96	20.6	0.662	85.27	196	w.o.	3-1/2
37	X		200	124	97	20.6	0.662	85.27	196	w.o.	3-1/2
37	X		201.8	121.2	83.8	21.7	0.662	85.27	196	w.o.	4-1/2
34		X	196.5	126	100	21.6	0.684	85.36	N/A	w.o.	3-1/2
34		X	197.2	123.5	97	22.1	0.684	85.36	N/A	w.o.	4
34		X	196.5	114.3	89	23.6	0.684	85.36	N/A	w.o.	4-1/2
34		X	197.2	114.3	80.5	23.6	0.684	85.36	N/A	w.o.	5-1/2
35		X	195	123	95	21.3	0.772	85.98	N/A	w.o.	3-1/2
35		X	195	113	83.2	23.2	0.772	85.98	N/A	w.o.	4-1/2
35		X	195.2	113	75.5	23.2	0.772	85.98	N/A	w.o.	5-1/2
35		X	195.2	113	70	23.2	0.772	85.98	N/A	w.o.	6-1/2

Table A1. Early test results - Carbon Monoxide (continued).

Run #	Saturated	Unsaturated	Helium					T K	V5		V23 Position (turns open)
			P ₁ atm	P ₂ atm	P ₃ atm	ΔP ₄ psi	P _{sat} atm		Saturation Pressure atm	Position (turns open)	
39	X		197	115.5	50	21.1	0.704	196	w.o.	5-1/2	
39	X		198	115.5	76	20	0.704	196	w.o.	5-1/2	
39	X		198	120.5	77.5	21.8	0.704	196	w.o.	5-1/2	
39	X		198	75.2	64.5	10.6	0.704	196	w.o.	5-1/2	
39	X		199	65	60	5.5	0.704	196	w.o.	5-1/2	
39	X		199	71	63	8.8	0.704	196	w.o.	5-1/2	
39	X		198.5	120.2	78	21.9	0.704	196	w.o.	5-1/2	
39	X		198	116	77	21.1	0.704	196	w.o.	5-1/2	
39	X		198	109	76	19.9	0.704	196	w.o.	5-1/2	
39	X		199	104	72	19.1	0.704	196	w.o.	5-1/2	
39	X		199	98	73	17.9	0.704	196	w.o.	5-1/2	
39	X		199	91	65	16.8	0.704	196	w.o.	7-1/2	
40		X	173	123	40	24.07	0.675	N/A	w.o.	5-1/2	
40	X		158	112.9	42.7	21.63	0.675	N/A	w.o.	5-1/2	
40	X		160	113	46.2	21.78	0.675	N/A	w.o.	5-1/2	
40	X		160.5	114.3	70.3	22.08	0.675	N/A	w.o.	5-1/2	
40	X		158	116	64.8	21.88	0.675	N/A	w.o.	5-1/2	
40	X		144.8	102.7	74	19.48	0.675	N/A	w.o.	5-1/2	
40	X		151.2	108.3	75.5	20.70	0.675	N/A	w.o.	5-1/2	
40	X		135	95.2	73	17.73	0.675	N/A	w.o.	5-1/2	
40	X		122.8	89.5	69	13.76	0.675	N/A	w.o.	5-1/2	
40	X		110.5	82.5	66.5	10.90	0.675	N/A	w.o.	5-1/2	
40	X		145.8	104.1	74.7	19.61	0.675	N/A	w.o.	5-1/2	
40	X		140.8	98.7	74	18.60	0.675	N/A	w.o.	5-1/2	
40	X		150.3	106.7	76	20.47	0.675	N/A	w.o.	5-1/2	
40	X		168.2	122.2	78.7	23.33	0.675	N/A	w.o.	5-1/2	
40	X		164.3	117.3	77.8	22.88	0.675	N/A	w.o.	5-1/2	

ORIFICE upstream of V-5 REMOVED AFTER #40

Appendix A2

The throttling orifice upstream of V5 was removed for all runs in Table A2, and the required pressure drop upstream from the venturi was provided by throttling through valve V5. All of the runs in Table A2 except 56-59 were "burst tests" in which either valve V5 or V23 was varied during the test while all other test parameters were held constant. The objective of these tests was to investigate the effects (on flow) of varying the pressure upstream and downstream from the venturi for neat fluids and fluids saturated with helium.

Table A2. Final test results - Carbon Monoxide.

Run #	Saturated	Unsaturated	P ₁ atm*	P ₂ atm	P ₃ atm	ΔP ₄ psi	P _{sat} atm	T K	Helium Saturation Pressure g _{atm}	V5 Position (turns open)	V23 Position (turns open)
41		X	129.6	120	39.2	22.25	0.670	85.32	N/A	w.o.	6
41		X	131	120	59.3	22.25	0.670	85.32	N/A	w.o.	6
41		X	132.3	77.3	62.2	10.42	0.670	85.32	N/A	1/2	6
41		X	132.7	117.2	75.3	22.10	0.670	85.32	N/A	1	6
41		X	133.4	110.3	74.1	20.87	0.670	85.32	N/A	3/4	6
41		X	134	107.8	73.9	20.29	0.670	85.32	N/A	3/4	6
41		X	134	105.9	72.7	20.00	0.670	85.32	N/A	3/4	6
41		X	134	103	72.2	19.40	0.670	85.32	N/A	3/4	6
41		X	134.3	98	71.2	18.51	0.670	85.32	N/A	3/4	6
41		X	134	93	70.2	17.62	0.670	85.32	N/A	3/4	6
41		X	134	86.8	66.8	14.12	0.670	85.32	N/A	3/4	6
41		X	134.2	121.2	77.9	22.51	0.670	85.32	N/A	~1/2	6
41		X	134.2	121	86.2	22.88	0.670	85.32	N/A	w.o.	4-1/2
41		X	134.2	121	85	22.69	0.670	85.32	N/A	w.o.	5
41		X	131	123.7	99.3	15.48	0.670	85.32	N/A	w.o.	3
41		X	134.2	122.8	92.2	20.21	0.670	85.32	N/A	w.o.	4
42	X		132.7	118	69.4	20.52	0.670	85.32	120.	w.o.	6
42	X		132.7	114.7	69	20.05	0.670	85.32	120.	w.o.	6
42	X		132.7	110.2	68.4	19.25	0.670	85.32	120	3/4	6
42	X		132.7	111	68.3	19.13	0.670	85.32	120.	3/4	6
42	X		132.7	106.6	68	18.27	0.670	85.32	120.	3/4	6
42	X		132.9	107.1	68.1	18.52	0.670	85.32	120	3/4	6
42	X		133	103.7	66.8	17.82	0.670	85.32	120	3/4	6
42	X		133	99.2	66.2	17.10	0.670	85.32	120	3/4	6
42	X		133	90.9	64.2	15.26	0.670	85.32	120	3/4	6
42	X		134	77.3	59.9	10.88	0.670	85.32	120	~1/2	6
42	X		134	119.2	71.2	21.12	0.670	85.32	120	w.o.	6
42	X		134	122.3	99.8	15.29	0.670	85.32	120	w.o.	3

* all pressures recorded as atm are gage pressure

Table A2. Final test results - Nitrogen.

Run #	Saturated	Unsaturated	P ₁ atm	P ₂ atm	P ₃ atm	ΔP ₄ psi	P _{sat} atm	T K	Helium Saturation Pressure atm	V5 Position (turns open)	V23 Position (turns open)
43	X		128.3	116.1	77.5	20.60	0.546	80.22	123	w.o.	6
43	X		128.3	116	80.2	20.82	0.546	80.22	123	w.o.	6
43	X		126.8	113.3	80	20.43	0.546	80.22	123	w.o.	6
43	X		127.3	107.8	77.8	19.19	0.546	80.22	123	3/4	6
43	X		127.6	104	76.2	18.17	0.546	80.22	123	3/4	6
43	X		127.6	101.3	74.8	17.50	0.546	80.22	123	3/4	6
43	X		127.6	101.2	74.3	17.50	0.546	80.22	123	3/4	6
43	X		127.8	98.2	72.8	16.42	0.546	80.22	123	3/4	6
43	X		127.6	89.8	69.6	14.22	0.546	80.22	123	~1/2	6
43	X		128.1	114.1	79.2	20.62	0.546	80.22	123	w.o.	6
43	X		128.1	118.2	99.7	13.92	0.546	80.22	123	w.o.	3
44		X	127.3	114.3	77.8	21.68	0.574	80.33	N/A	w.o.	6
44	X		123	109	77.8	20.53	0.574	80.33	N/A	w.o.	6
44	X		124.7	110.2	78	20.78	0.574	80.33	N/A	w.o.	6
44	X		127.6	112.7	78.3	21.37	0.574	80.33	N/A	3/4	6
44	X		127.8	108.1	77.5	20.60	0.574	80.33	N/A	3/4	6
44	X		127.8	107.9	77.1	20.50	0.574	80.33	N/A	3/4	6
44	X		127.8	106.2	76.8	20.23	0.574	80.33	N/A	3/4	6
44	X		128.3	104	76.2	19.55	0.574	80.33	N/A	3/4	6
44	X		128.3	101	74.8	18.92	0.574	80.33	N/A	3/4	6
44	X		128.3	98.2	74.3	18.72	0.574	80.33	N/A	3/4	6
44	X		128.3	97.8	74.1	18.49	0.574	80.33	N/A	3/4	6
44	X		128.3	90.7	71.2	16.56	0.574	80.33	N/A	~1/2	6
44	X		128.3	83.2	68.6	13.32	0.574	80.33	N/A	w.o.	6
44	X		128.3	118.1	100.8	14.56	0.574	80.33	N/A	w.o.	3

Table A2. Final test results - Nitrous Oxide.

Run #	Saturated	Unsaturated	P ₁ atm	P ₂ atm	P ₃ atm	ΔP ₄ psi	P _{sat} atm	T K	Helium Saturation Pressure atm	V5 Position (turns open)	V23 Position (turns open)
46		X	90.7	83.9	35.1	13.27	18.6	255.3	N/A	w.o.	6
46		X	90.7	81.5	35.9	12.47	18.6	255.3	N/A	w.o.	6
46		X	91.1	74.3	36.6	10.70	18.6	255.3	N/A	3/4	6
46		X	91.1	75.7	39.4	10.82	18.6	255.3	N/A	3/4	6
46		X	91.4	70.2	41.6	9.75	18.6	255.3	N/A	3/4	6
46		X	91.6	76.9	46.4	11.03	18.6	255.3	N/A	7/8	6
46		X	91.8	73.5	49.4	10.50	18.6	255.3	N/A	7/8+	6
46		X	91.8	86.4	71.1	10.18	18.6	255.3	N/A	w.o.	3
46		X	91.8	82.3	63.0	13.02	18.6	255.3	N/A	w.o.	4
46		X	91.8	85.2	64.2	12.98	18.6	255.3	N/A	w.o.	4
46		X	92.2	85.3	67.5	12.62	18.6	255.3	N/A	w.o.	3.5
46		X	91.8	85.3	50.9	13.03	18.6	255.3	N/A	w.o.	6
48			86.8	81.2	51.6	11.22	18.5	254.9	75	w.o.	6
48	X		87.6	80.7	50.6	10.87	18.5	254.9	75	1-1/4	6
48	X		87.6	78.6	50.2	10.15	18.5	254.9	75	1-1/4	6
48	X		87.6	76.4	50.2	9.70	18.5	254.9	75	7/8	6
48	X		87.6	75.2	59.6	9.08	18.5	254.9	75	3/4	6
48	X		87.7	74.4	49.3	8.82	18.5	254.9	75	3/4	6
48	X		88.0	73.1	49.1	8.58	18.5	254.9	75	3/4	6
48	X		88.0	70.5	48.2	8.02	18.5	254.9	75	~1/2	6
48	X		88.0	82.5	69.1	8.47	18.5	254.9	75	w.o.	3
52		X	73.5	67.8	47.6	8.13	25.2	266.3	N/A	w.o.	6
52	X		74.2	68.1	47.4	8.32	25.2	266.3	N/A	w.o.	6
52	X		81.2	73.7	48.8	9.31	25.2	266.3	N/A	w.o.	6
52	X		75.6	68.5	48.1	8.24	25.2	266.3	N/A	w.o.	6
52	X		75.6	67.2	48.0	8.10	25.2	266.3	N/A	1-1/8	6
52	X		75.6	64.3	47.6	7.80	25.2	266.3	N/A	7/8	6
52	X		75.3	64.3	47.0	7.62	25.2	266.3	N/A	3/4	6
52	X		75.2	63.2	46.8	7.39	25.2	266.3	N/A	3/4	6
52	X		75.3	61.1	46.7	7.03	25.2	266.3	N/A	3/4	6
52	X		75.2	60.5	46.6	6.88	25.2	266.3	N/A	~1/2	6
52	X		75.2	69.2	60.7	6.06	25.2	266.3	N/A	w.o.	3
52	X		75.2	68.2	57.1	8.00	25.2	266.3	N/A	w.o.	4
52	X		75.1	68.0	51.5	8.13	25.2	266.3	N/A	w.o.	5
52	X		75.1	68.0	48.4	8.22	25.2	266.3	N/A	w.o.	6

Table A2. Final test results - Nitrous Oxide (continued).

Run #	Saturated	Unsaturated	P ₁ atm	P ₂ atm	P ₃ atm	ΔP ₄ psi	P _{sat} atm	T K	Helium Saturation Pressure atm	V5 Position (turns open)	V23 Position (turns open)
53	X		75.8	70.1	48.4	7.20	25.2	266.1	75.2	w.o.	6
53	X		75.7	68.8	48.3	6.98	25.2	266.1	75.2	1-1/8	6
53	X		75.7	68.4	48.4	6.80	25.2	266.1	75.2	1	6
53	X		75.7	68.1	48.3	6.63	25.2	266.1	75.2	7/8	6
53	X		75.8	66.6	47.6	6.35	25.2	266.1	75.2	3/4	6
53	X		75.7	64.8	47.0	6.02	25.2	266.1	75.2	3/4	6
53	X		75.8	66.1	47.4	6.20	25.2	266.1	75.2	3/4	6
53	X		75.7	64.4	47.3	6.00	25.2	266.1	75.2	3/4	6
53	X		75.8	62.2	46.2	5.63	25.2	266.1	75.2	3/4	6
53	X		75.8	70.2	55.7	6.82	25.2	266.1	75.2	w.o.	4
53	X		75.9	69.8	51.9	7.04	25.2	266.1	75.2	w.o.	5
56		X	75.2	69.8	47.0	8.55	25.2	266	N/A	w.o.	6
58		X	75.6	71.1	45.5	8.82	25.2	266	N/A	w.o.	6
60		X	75.8	70.7	48.0	8.53	25.2	266	N/A	w.o.	6
57	X		76.3	71.8	56.3	7.45	25.2	266	75.5	w.o.	6
59	X		75.8	71.2	49.4	7.45	25.2	266	75.5	w.o.	6
54	X		78.2	72.3	48.6	9.43	12.6	243.9	79.3	w.o.	6
54	X		75.8	69.7	48.6	8.80	12.6	243.9	79.3	w.o.	6
54	X		76.0	68.6	48.6	8.70	12.6	243.9	79.3	1-1/8	6
54	X		75.9	66.5	48.0	8.70	12.6	243.9	79.3	1	6
54	X		75.8	65.2	47.6	7.90	12.6	243.9	79.3	7/8	6
54	X		75.8	64.3	47.6	7.67	12.6	243.9	79.3	3/4	6
54	X		78.2	66.2	48.0	8.22	12.6	243.9	79.3	3/4	6
54	X		78.2	63.6	47.5	7.63	12.6	243.9	79.3	3/4	6
54	X		78.2	60.1	46.4	7.06	12.6	243.9	79.3	~1/2	6
54	X		78.2	70.7	53.6	9.41	12.6	243.9	79.3	w.o.	5
54	X		78.2	72.5	59.2	8.92	12.6	243.9	79.3	w.o.	4
54	X		78.5	73.7	64.2	6.70	12.6	243.9	79.3	w.o.	3
54	X		78.5	68.6	49.7	8.80	12.6	243.9	79.3	w.o.	6
54	X		78.2	71.7	50.6	9.60	12.6	243.9	79.3	w.o.	6

Table A2. Final test results - Nitrous Oxide (continued).

Run #	Saturated	Unsaturated	P ₁ atm	P ₂ atm	P ₃ atm	ΔP ₄ psi	P _{sat} atm	T K	Helium Saturation Pressure atm	V5 Position (turns open)	V23 Position (turns open)
55		X	77.5	71.1	48.5	10.72	12.8	244.1	N/A	w.o.	6
55		X	77.5	69.8	49.5	10.40	12.8	244.1	N/A	1-1/8	6
55		X	77.4	67.3	48.9	10.03	12.8	244.1	N/A	1-1/8	6
55		X	77.5	66.5	48.9	9.87	12.8	244.1	N/A	7/8	6
55		X	77.6	63.6	48.2	9.38	12.8	244.1	N/A	3/4	6
55		X	77.6	61.2	47.9	8.72	12.8	244.1	N/A	5/8	6
55		X	77.6	60.7	47.8	8.70	12.8	244.1	N/A	1/2	6
55		X	77.6	57.8	46.9	8.00	12.8	244.1	N/A	1/2	6
55		X	77.7	70.8	54.3	10.53	12.8	244.1	N/A	w.o.	5
55		X	77.7	71.6	58.1	9.03	12.8	244.1	N/A	w.o.	4
55		X	77.7	72.2	60.3	8.12	12.8	244.1	N/A	w.o.	3-1/2
55		X	77.7	70.9	56.6	10.12	12.8	244.1	N/A	w.o.	4-1/2

U.S. DEPT. OF COMM. BIBLIOGRAPHIC DATA SHEET	1. PUBLICATION OR REPORT NO. NBSIR 75-806	2. Gov't Accession No.	3. Recipient's Accession No.
4. TITLE AND SUBTITLE PHASE EQUILIBRIUM AND FLOW-INDUCED DESORPTION DATA FOR He-CO, He-N ₂ O, and He-N ₂ SYSTEMS		5. Publication Date February 1975	6. Performing Organization Code
7. AUTHOR(S) W. G. Steward, R.O. Voth, J. Hord, W.R. Parrish, C. F. Sindt, J.M. Arvidson	8. Performing Organ. Report No.		
9. PERFORMING ORGANIZATION NAME AND ADDRESS NATIONAL BUREAU OF STANDARDS DEPARTMENT OF COMMERCE WASHINGTON, D.C. 20234		10. Project/Task/Work Unit No. 2750559	11. Contract/Grant No. AF/Kirtland No. AFWL 75-177
12. Sponsoring Organization Name and Complete Address (Street, City, State, ZIP) Kirtland Air Force Base Albuquerque, New Mexico 87117		13. Type of Report & Period Covered Final	14. Sponsoring Agency Code
15. SUPPLEMENTARY NOTES			
16. ABSTRACT (A 200-word or less factual summary of most significant information. If document includes a significant bibliography or literature survey, mention it here.) Liquid-vapor equilibrium data were obtained for the helium-carbon monoxide and helium-nitrous oxide systems at pressures to 138 bars. Liquid and vapor phase compositions were measured at nominal temperatures of 80, 85, 90, 100, and 120 K (144, 153, 162, 180, and 216°R) for the helium-carbon monoxide system, and at 235, 245, 265, and 285 K (423, 441, 477, and 513°R) for the helium-nitrous oxide system. Internal consistency of the data was checked by using pseudo-Henry's law constants and enhancement factors. The effects on flow of helium absorption and subsequent flow-induced desorption were investigated by means of reduced scale model experiments. Friction losses attributable to helium desorption in the long channels proved to be negligible both in experimental measurements and in calculations based on assumed equilibrium of liquid and gas. Contrarily, the assumption of phase equilibrium leads to gross miscalculations of flow rates in cavitating or near cavitating nozzles or venturis. Actual venturi mass flow rates reached in the experiments were fifty times the theoretical choking flow rates; however, definite mass flow rate reductions due to helium desorption were measured, ranging from four percent for nitrogen to twelve percent for nitrous oxide. Pertinent experiences in handling these fluids and operating the test equipment are also discussed.			
17. KEY WORDS (six to twelve entries; alphabetical order; capitalize only the first letter of the first key word unless a proper name; separated by semicolons) Binary mixture; cavitating venturi; enhancement factors; experimental vapor-liquid equilibria; flow induced desorption; helium-carbon monoxide system; helium-nitrous oxide system; Henry's law constants; two phase choking; two phase flow.			
18. AVAILABILITY <input checked="" type="checkbox"/> Unlimited <input type="checkbox"/> For Official Distribution. Do Not Release to NTIS <input type="checkbox"/> Order From Sup. of Doc., U.S. Government Printing Office Washington, D.C. 20402, SD Cat. No. C13 <input type="checkbox"/> Order From National Technical Information Service (NTIS) Springfield, Virginia 22151	19. SECURITY CLASS (THIS REPORT) UNCLASSIFIED	21. NO. OF PAGES	
		20. SECURITY CLASS (THIS PAGE) UNCLASSIFIED	22. Price

